AGU PUBLICATIONS

Paleoceanography

RESEARCH ARTICLE
10.1002/2013PA002570

Key Points:
- Deep water formed in the N Pacific during HS1 reaching 3600 m
- Driven by reduced atmospheric freshwater flux during stadial conditions
- Model shows that N Pacific deep water can account for significant deglacial CO_2 rise

Supporting Information:
- Text S1
- Table S1
- Figure S1
- Figure S2
- Figure S3
- Figure S4
- Figure S5

Correspondence to:
J. W. B. Rae,
jwbr@st-andrews.ac.uk

Citation:
Rae, J. W. B., M. Sarnthein, G. L. Foster, A. Ridgwell, P. M. Grootes, and T. Elliott (2014), Deep water formation in the North Pacific and deglacial CO_2 rise, *Paleoceanography*, *29*, 645–667, doi:10.1002/2013PA002570.

Received 7 OCT 2013
Accepted 23 MAY 2014
Accepted article online 1 JUN 2014
Published online 27 JUN 2014

Deep water formation in the North Pacific and deglacial CO_2 rise

James W. B. Rae[1,2,3,4], Michael Sarnthein[5], Gavin L. Foster[6], Andy Ridgwell[2], Pieter M. Grootes[7], and Tim Elliott[1]

[1]Bristol Isotope Group, Department of Earth Sciences, University of Bristol, Bristol, UK, [2]BRIDGE, School of Geographical Sciences, University of Bristol, Bristol, UK, [3]Division of Geological and Planetary Sciences, California Institute of Technology, Pasadena, USA, [4]Department of Earth and Environmental Sciences, University of St Andrews, St Andrews, UK, [5]Institut für Geowissenschaften, University of Kiel, Kiel, Germany, [6]Ocean and Earth Science, National Oceanography Centre Southampton, University of Southampton, Southampton, UK, [7]Institute of Ecosystem Research, University of Kiel, Kiel, Germany

Abstract Deep water formation in the North Atlantic and Southern Ocean is widely thought to influence deglacial CO_2 rise and climate change; here we suggest that deep water formation in the North Pacific may also play an important role. We present paired radiocarbon and boron isotope data from foraminifera from sediment core MD02-2489 at 3640 m in the North East Pacific. These show a pronounced excursion during Heinrich Stadial 1, with benthic-planktic radiocarbon offsets dropping to ~350 years, accompanied by a decrease in benthic $\delta^{11}B$. We suggest that this is driven by the onset of deep convection in the North Pacific, which mixes young shallow waters to depth, old deep waters to the surface, and low-pH water from intermediate depths into the deep ocean. This deep water formation event was likely driven by an increase in surface salinity, due to subdued atmospheric/monsoonal freshwater flux during Heinrich Stadial 1. The ability of North Pacific Deep Water (NPDW) formation to explain the excursions seen in our data is demonstrated in a series of experiments with an intermediate complexity Earth system model. These experiments also show that breakdown of stratification in the North Pacific leads to a rapid ~30 ppm increase in atmospheric CO_2, along with decreases in atmospheric $\delta^{13}C$ and $\Delta^{14}C$, consistent with observations of the early deglaciation. Our inference of deep water formation is based mainly on results from a single sediment core, and our boron isotope data are unavoidably sparse in the key HS1 interval, so this hypothesis merits further testing. However, we note that there is independent support for breakdown of stratification in shallower waters during this period, including a minimum in $\delta^{15}N$, younging in intermediate water ^{14}C, and regional warming. We also re-evaluate deglacial changes in North Pacific productivity and carbonate preservation in light of our new data and suggest that the regional pulse of export production observed during the Bølling-Allerød is promoted by relatively stratified conditions, with increased light availability and a shallow, potent nutricline. Overall, our work highlights the potential of NPDW formation to play a significant and hitherto unrealized role in deglacial climate change and CO_2 rise.

1. Introduction

During the last deglaciation, atmospheric CO_2 levels rose in a series of steps, associated with millennial-scale shifts in global climate [*EPICA*, 2004; *Shakun et al*., 2012]. The magnitude and pacing of CO_2 rise point to the deep ocean as the dominant source of carbon [*Broecker*, 1982], and changes in deep water formation are commonly invoked to explain the release of this carbon to the atmosphere [e.g., *Knox and McElroy*, 1984; *Sarmiento and Toggweiler*, 1984; *Siegenthaler and Wenk*, 1984; *Sigman et al*., 2010; *Sarnthein et al*., 2013]. At the present day, deep water formation to depths greater than 2000 m takes place in the North Atlantic and Southern Oceans, and mechanisms to explain deglacial climate and CO_2 change have thus focused on these regions [*Toggweiler et al*., 2006; *Hain et al*., 2010]. A paradigm has emerged [*Denton et al*., 2010] that invokes reduced North Atlantic Deep Water formation as a mechanism for driving cold stadial periods in the Northern Hemisphere [*Sarnthein et al*., 2001; *McManus et al*., 2004], such as Henrich Stadial 1 (HS1 ~ 19–14.7 ka) and the Younger Dryas (YD 12.9–11.8 ka). At these times, the Southern hemisphere is observed to warm [*Barker et al*., 2009; *Pedro et al*., 2011], and this "bipolar seesaw" of temperature change is thought to be associated with shifts in atmospheric circulation [*Fletcher and Moreno*, 2011] and sea ice cover [*Fischer et al*., 2007]. These in turn may cause reduced stratification in the Southern Ocean, with increased upwelling bringing carbon-rich

deep waters to the surface [*Anderson et al*., 2009]. Given the inefficiency of phytoplankton productivity in the Southern Ocean, CO_2 and nutrients brought to the surface by deep mixing are not fully utilized by photosynthesis [*François et al*., 1997], and CO_2 may thus escape from the deep ocean to the atmosphere [*Toggweiler et al*., 2006; *Sigman et al*., 2010].

The role of the North Pacific in this deglacial chain of events has been thought to be less active than those of its polar siblings, the North Atlantic and Southern Ocean [*Haug and Sigman*, 2009]. In contrast to the North Atlantic and Southern Oceans, the North Pacific does not currently form deep water, due to regional density stratification caused by low salinity in surface waters (Figure 1) [*Warren*, 1983; *Emile-Geay et al*., 2003; *Ferreira et al*., 2010]. Although several studies have suggested that North Pacific intermediate water formation increased during glacial and stadial conditions [*Kennett and Ingram*, 1995; *Keigwin*, 1998; *Matsumoto et al*., 2002; *Herguera et al*., 2010; *Okazaki et al*., 2010], it has been assumed that this did not penetrate deeper than ~2700 m. Thus, while the deep North Pacific has been considered an efficient glacial CO_2 store [*Galbraith et al*., 2007], it has not previously been thought to form deep water or to play a direct role in deglacial CO_2 rise [*Haug and Sigman*, 2009].

We challenge this view with new data from sediment core MD02-2489 from the deep North Eastern Pacific. We use coupled measurements of the boron isotope ($\delta^{11}B$) and radiocarbon (^{14}C) composition of foraminifera to trace the chemistry of carbon in the deep North Pacific and its exchange with the atmosphere over the last deglaciation. These data are interpreted with support from an Earth system model and compared to regional proxy data, to provide a new picture of deglacial circulation in the North Pacific, and its role in atmospheric CO_2 rise.

2. Regional Setting

2.1. Circulation

The deep North Pacific is ventilated, today, by derivatives of waters from the Southern Ocean and North Atlantic [*Reid*, 1969; *Broecker et al*., 1998; *Tomczak and Godfrey*, 1994]. These waters gradually de-densify, upwell, and recirculate southward at mid-depths of the Pacific, creating a large body of old and weakly stratified deep water [*Warren and Owens*, 1988; *Reid*, 1997; *Emile-Geay and Madec*, 2008]. Local ventilation in the North Pacific is currently limited to intermediate depths (~300–800 m) [*Talley*, 1993]. This North Pacific Intermediate Water forms through winter cooling and brine rejection in the Sea of Okhotsk [*Talley*, 1991; *Yasuda et al*., 2002; *Shcherbina et al*., 2003], and perhaps also the Alaskan Gyre [*Van Scoy et al*., 1991], with further modification by subsurface mixing in the Kurile Islands and Kuroshio and Oyashio currents [*Talley*, 1997]. The density (and hence depth penetration) of these locally ventilated waters is strongly limited by low sea surface salinity in the subpolar gyre [*Warren*, 1983]. Although the surface of the northern North Pacific cools to near freezing in the Winter, salinity is only 32.8, significantly lower than underlying deep water salinities of 34.6 (c.f. equivalent values of 34.7 and 34.9 in the northern North Atlantic; Figure 1a) [*Emile-Geay et al*., 2003].

The causes of the subpolar North Pacific salinity minimum, and associated stratification, are thoroughly reviewed by *Warren* [1983] and *Emile-Geay et al*. [2003], who highlight the local excess of precipitation over evaporation, combined with minimal exchange of subpolar waters with the relatively salty subtropical gyre. This local precipitation occurs mainly in the Westerly storm track, which transfers water vapor from low latitudes and the East Asian Monsoon region to the subpolar gyre [*Emile-Geay et al*., 2003]. Other freshwater inputs include monsoonal run-off [*Wang et al*., 2005] and transfer in the trade winds of moisture evaporated from the Atlantic [*Broecker et al*., 1985]. The minimal exchange of water between the subtropical and subpolar gyres is a function of the relatively zonal wind stress in the North Pacific, and the lack of large-scale overturning circulation [*Emile-Geay et al*., 2003; *Stommel*, 1961]. Although some aspects of Pacific freshness are related to basin geometry [*Ferreira et al*., 2010; *Nilsson et al*., 2013] and will thus remain constant on glacial-interglacial timescales, the influences of major rain belts and cross-gyre exchange have the potential to change dynamically, and may thus drive significant changes in sea surface salinity and deep water formation in the past [e.g., *Boyle and Keigwin*, 1987; *Okazaki et al*., 2010].

2.2. Biogeochemistry

The subpolar North Pacific surface is a High Nutrient Low Chlorophyll zone, with abundant major nutrients that are not efficiently used by phytoplankton. Major nutrients are supplied to the surface by intense winter

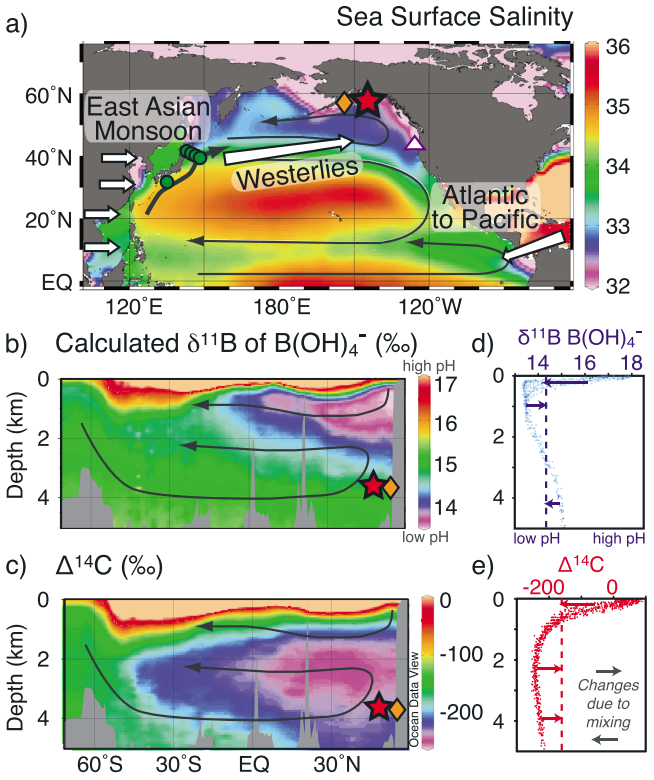

Figure 1. Modern North Pacific circulation and biogeochemistry [*Schlitzer*, 2004]. (a) Annual average sea surface salinity from the WOA09 database [*Antonov et al.*, 2010]. The location of our core MD02-2489, 54.39°N, 148.92° W, 3640 m is shown with a red star, ODP 887 (54.37°N, 148.45°W, 3647 m) [*Galbraith et al.*, 2007] with an orange diamond, W8709A-13PC (42.1°N, 125.8°W, 2710 m) [*Lund et al.*, 2011a, 2011b] with a white triangle, and the *Okazaki et al.* [2010] NW Pacific compilation with green circles. Note that the symbols for MD02-2489 and ODP 887 should plot on top of one another, and so have been separated for legibility. White arrows indicate input of freshwater to the North Pacific from the Westerly storm track, the tropical Atlantic, and rivers and precipitation fed by the East Asian Monsoon [*Emile-Geay et al.*, 2003]. Black arrows indicate average modern circulation patterns [*Tomczak and Godfrey*, 1994]. Input of freshwater from the atmosphere, combined with the relative isolation of the subpolar gyre, gives low sea surface salinity in the North Pacific, and creates stratified conditions. (b) Water column $\delta^{11}B$ of $B(OH)_4^-$, calculated from GLODAP carbonate system data [*Key et al.*, 2004], using α_B of 27.2‰ [*Klochko et al.*, 2006], $\delta^{11}B_{SW}$ of 39.61‰ [*Foster et al.*, 2010], $[B]_T$ of 432.6 µmol/kg [*Lee et al.*, 2010], and CO2SYS.m [*van Heuven et al.*, 2009], with parameters as recommended by *Dickson et al.* [2007]. This property follows pH and is recorded by benthic foraminifera [*Rae et al.*, 2011]; see also Figure S1. (c) Water column $\Delta^{14}C$ from GLODAP, with no correction for bomb radiocarbon. Sections are averaged from 150°W to 170°W, and black arrows indicate modern overturning circulation. Profiles in Figures 1d and 1e show water column data in the region of our core site, from 135°W to 160°W and 40°N to 60°N. Note that our core site (red star) is bathed by some of the most ^{14}C-depleted (low $\Delta^{14}C$) waters in the ocean (c and e) and underlies an extensive region of low $\delta^{11}B$ of $B(OH)_4^-$ (low pH) at intermediate depths (b and d). Local convective mixing during deep water formation (schematic arrows in Figures 1d and 1e) would thus work to bring young, low pH waters to the depth of our core.

cyclones, alongside extensive upwelling driven by cyclonic wind stress curl in the subpolar gyre and tidal mixing in the Kurile Island chain [*Nakamura et al.*, 2000; *Sarmiento et al.*, 2004; *Tsunogai*, 2002; *Key et al.*, 2004]. Given the abundance of major nutrients in this region, phytoplankton productivity is limited by light and minor nutrients, such as iron [*Boyd et al.*, 2007].

At intermediate depths, North Pacific biogeochemistry is characterized by an extensive oxygen minimum zone. These waters also have extremely low pH, due to remineralization of organic carbon into dissolved inorganic carbon (DIC) (Figures 1 and S1). Below depths of ~1800 m, pH increases due to remineralization of $CaCO_3$, which occurs deeper in the water column than organic carbon, and provides a source of alkalinity to deep waters (Figure S1).

Radiocarbon has a notably different profile than pH, being predominantly controlled by ventilation age, with minimal influence from remineralization. As a result, depths of ~200–500 m have relatively young radiocarbon ages but extremely low pH. In contrast, at the depth of the sediment core described in this study (3640 m), radiocarbon ages are among the oldest in the water column, whereas pH is significantly higher than that at intermediate depths (Figure 1).

3. Methods

Sediment core MD02-2489 was raised from 3640 m on the Patten Seamount off the Alaskan Margin at 54.39° N, 148.92° W (Figure 1). Its sedimentology is thoroughly described by Gebhardt et al. (2008; their supplementary Figure 2) and shows no notable disturbance (slumping, burrowing, etc.) during the deglaciation, though there is some evidence of coring disturbance in the top 50 cm of the core, which prevented us from making core-top measurements. The high sedimentation rate (~20 cm/kyr) and availability of epifaunal benthic foraminifera in MD02-2489 are rare

attributes in cores of this depth in the North Pacific and make MD02-2489 particularly well-suited to this study.

3.1. Age Control

In this study we establish a new age model for MD02-2489 based on correlation of high-resolution (2 cm sample spacing) $\delta^{18}O$ from planktic foraminifera [*Gebhardt et al*., 2008] to $\delta^{18}O$ from the NGRIP ice core [*NGRIPmembers*, 2004; *Johnsen et al*., 1997] on the GICC05 timescale [*Rasmussen et al*., 2006; *Andersen et al*., 2006; *Svensson et al*., 2006] and $\delta^{18}O$ from Hulu Cave speleothem records [*Wang et al*., 2001; *Southon et al*., 2012; *Wu et al*., 2009] (Figure S2 and Table S1). The $\delta^{18}O$ features in our data and reference records may be related by: (1) a salinity link between the East Asian Monsoon and North Pacific surface waters [*Wang et al*., 1999]; (2) a temperature link between Greenland and the North Pacific [*Hendy and Kennett*, 2000; *Kiefer et al*., 2001; *Shen et al*., 2010]; and/or (3) a North Pacific source of precipitation at NGRIP, especially under glacial conditions [*Kiefer et al*., 2002; *Langen and Vinther*, 2009]. We note that correlation to either the speleothem or the ice core reference records produces a very similar chronology for our core, and that the removal of either record, or any individual tie point, would have little effect on our age model. The youngest portion of our core (13–6 ka) lacks distinct tie points. We thus use conventional radiocarbon dating in this interval, with the Marine09 curve from IntCal09 [*Reimer et al*., 2009], and a reservoir age of 850 ± 100 years for the shallow subsurface habitat of *Neogloboquadrina pachyderma* (s.) [*Southon and Fedje*, 2003; *Hutchinson et al*., 2004; *Key et al*., 2004]. This approach is less risky in this interval than for the early deglacial, as deep ocean and atmospheric ^{14}C values are, by this time, much less disparate [*Robinson et al*., 2005; *Skinner et al*., 2010; *Burke and Robinson*, 2012], so changes in ocean circulation are less likely to significantly alter reservoir ages [*Southon and Fedje*, 2003; *Hutchinson et al*., 2004].

Age control in MD02-2489 has previously been established using planktic ^{14}C plateau tuning (a technique described by *Sarnthein et al*. [2007]) by *Gebhardt et al*. [2008], and this has been recently updated by *Sarnthein et al*. [2013] (Figure S3 and Table S2). Good agreement is seen between these independent approaches, both of which place the major excursion in our benthic-planktic ^{14}C offsets during early HS1 (Figure S3). Furthermore, many of our conclusions can be reached in "depth" space by comparing multiproxy data within our core MD02-2489 (Figure 2). Thus, choice of age model does not change the main conclusions of our study.

We also present an updated age model for ODP 887, which is adjacent to our core site. ODP 887's original deglacial age model [*Galbraith et al*., 2007] was based on conventional radiocarbon dating, assuming a reservoir age of 950 ± 200 years throughout the deglaciation; these age control points were then shifted within their uncertainties to give smooth variations in sedimentation rate. We have updated ODP 887's age model for the early deglaciation, based on ties between % $CaCO_3$ data at this site and in our adjacent core MD02-2489 (Figure S4, Table S3). This approach is supported by the close proximity of our sites: MD02-2489 is at 54.39°N, 148.92°W, 3640 m and ODP 887 is at 54.37°N, 148.45°W, 3647 m (see Figure 1). We note that this revised age model gives excellent agreement between % organic carbon records and planktic radiocarbon data (Figure S4) and gives smoother variations in ODP 887's sedimentation rate than in the published age model [*Galbraith et al*., 2007]. Furthermore, these tie points remain within the 2σ uncertainties of the published age control points. For the LGM and late deglacial portions of ODP887, we use conventional ^{14}C dating, as these intervals lack distinct tie points. We use the Marine09 curve from IntCal09 [*Reimer et al*., 2009], with a reservoir age of 1800 ± 250 years in the LGM, as constrained by reservoir ages in our core, and reservoir ages of 850 ± 100 years in the late deglacial, as used in our core during the late deglacial and Holocene. Note that, irrespective of the absolute chronology, our approach serves to synchronize these two cores.

3.2. Proxy Background and Analysis

3.2.1. Radiocarbon

The radiocarbon content of dissolved inorganic carbon (DIC) in seawater reflects the exchange of CO_2 at the ocean's surface with the atmosphere, and the subsequent radioactive decay of ^{14}C as deep water circulates within the ocean's interior. Radiocarbon content may be expressed as a ^{14}C age, or in $\Delta^{14}C$ units, which gives the $^{14}C/^{12}C$ ratio of a sample relative to a standard, and corrected for mass-dependent isotope fractionation and decay since time of sample formation. Planktic foraminifera record the ^{14}C content of waters in their

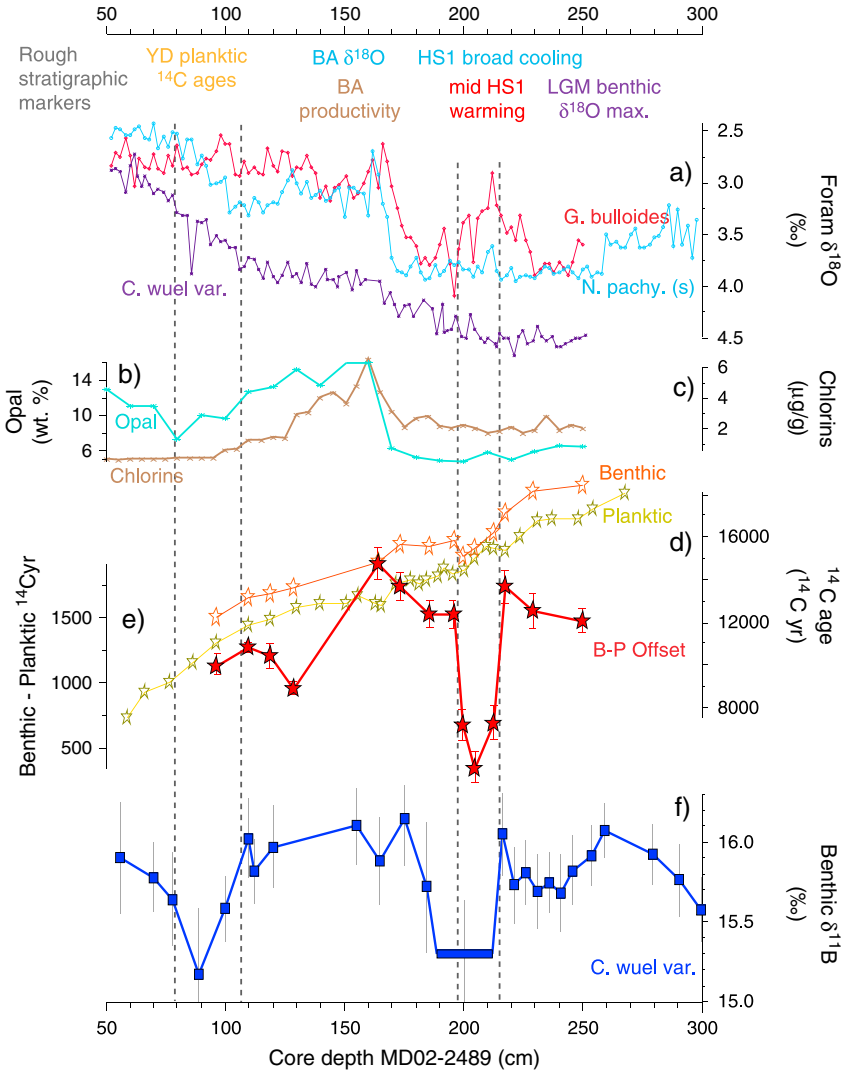

Figure 2. Proxy data from sediment core MD02-2489 plotted versus core depth [*Gebhardt et al.*, 2008] (and this study). Data include: (a) δ^{18}O of benthic and planktic foraminifera; (b) biogenic opal content; (c) chlorophyll pigment content; (d) ^{14}C age of benthic and planktic foraminifera; (e) benthic-planktic ^{14}C offsets; and (f) δ^{11}B of benthic foraminifera with 2 SD error bars. Rough stratigraphic indicators are given at the top of the figure, with abbreviations: LGM is Last Glacial Maximum (~21–19 ka), HS1 is Heinrich Stadial 1 (~19–14.7 ka), BA is Bølling-Allerød (14.7-12.9 ka), and YD is Younger Dryas (12.9–11.8 ka). Using δ^{18}O, the BA productivity spike [*Kohfeld and Chase*, 2011] and raw planktic ^{14}C ages to provide a rough measure of stratigraphy, we observe an excursion to low pH and a minimum in benthic-planktic ^{14}C offset during the early deglaciation, around HS1, and a second low-pH event later in the deglaciation, around the YD. The broad symbol in the δ^{11}B record indicates the wide temporal extent of this sample; all other samples span a similar temporal extent to the symbols.

surface (or shallow subsurface) habitat, which reflects the balance between CO_2 exchange with the atmosphere, and upwelling of ^{14}C-depleted waters from below. Benthic foraminifera record the ^{14}C content of ambient deep waters, a function of the time since that water left the surface ocean. A reduced ^{14}C offset between benthic and planktic foraminifera may thus act as a sensitive tracer of local deep water formation. Radiocarbon ventilation ages (or reservoir ages) are given here as the difference in ^{14}C age between foraminifera and the contemporaneous atmosphere (the ^{14}C content of which changes over time). We use the atmospheric ^{14}C compilation of IntCal09 [*Reimer et al.*, 2009], spliced with the Hulu Cave ^{14}C record for the 15–26 ka interval [*Southon et al.*, 2012]; reservoir ages associated with the plateau-tuned age model use the Lake Suigetsu ^{14}C record [*Ramsey et al.*, 2012]. Note that the foraminiferal ^{14}C reservoir ages given here are not equivalent to the true ventilation age of a parcel of water, as they are not calculated via the decay trajectory of ^{14}C [*Adkins and Boyle*, 1997], and because surface waters, when subducted, have a non-zero radiocarbon age.

Radiocarbon measurements were made on planktic foraminifera (*N. pachyderma* (s.)) and mixed benthic foraminifera (avoiding deep-dwelling infaunal species) [*Magana et al*., 2010] by Accelerator Mass Spectrometry (AMS), on graphite targets of foraminiferal carbonate. Given the sedimentation rate (~20 cm/kyr) and depth (3640 m) of MD02-2489, which results in low flux rates of particulate organic matter, mixing of ^{14}C signals by bioturbation is unlikely to be a significant issue [*Trauth et al*., 1997]. Benthic ^{14}C analyses were therefore made throughout the core, rather than limiting samples to benthic abundance peaks [see *Keigwin*, 2004]. Radiocarbon uncertainties are given at 1SE, in keeping with ^{14}C convention. Analytical uncertainties are around 30 ^{14}C years in the late Holocene, increasing to ~100 ^{14}C years at the LGM. $\Delta^{14}C$ error ellipses are based on a Monte Carlo simulation that combines age and analytical uncertainties and are typically ~70‰. The typical age range of tied features in our planktic $\delta^{18}O$ data and the reference ice core and speleothem records is of the order 200 calendar years; we thus use a calendar age uncertainty of 100 years (1 SD) for calculating uncertainty ellipses. Benthic-planktic uncertainties are based on the quadratic addition of analytical uncertainties in benthic and planktic ^{14}C, and are around 60 ^{14}C years in the late Holocene, and 150 ^{14}C years at the LGM (and see also *Sarnthein et al*. [2013]).

3.2.2. Boron Isotopes

The systematics of boron isotopes in benthic foraminifera are thoroughly described in *Rae et al*. [2011]. In brief, the boron isotope composition (expressed in $\delta^{11}B$ notation relative to NIST 951 standard) [*Catanzaro et al*., 1970] of epifaunal benthic foraminifera of the genus Cibicidoides has been shown to record the boron isotope composition of the borate ion ($B(OH)_4^-$) in seawater. As $\delta^{11}B$ of $B(OH)_4^-$ is a function of seawater pH, Cibicidoides $\delta^{11}B$ may be used to trace changes in the carbonate chemistry of bottom water at our core site (Figure S1).

Boron isotope analyses were made on samples of 9–25 (0.2–1.3 mg) oxidatively cleaned *Cibicidoides wuellerstorfi* var. by Multi-Collector Inductively Coupled Plasma Mass Spectrometry [*Foster*, 2008; *Rae et al*., 2011; *Foster et al*., 2013]. Uncertainty is reported at 95% confidence (2 SD) based on the relationship determined between sample size and long-term reproducibility, and in this data set is typically ~0.3‰ (equivalent to ~0.03 pH units) [*Rae et al*., 2011]. Samples for boron isotopes were typically picked from sediment core samples spanning 1 or 2 cm. However to obtain enough foraminifera, the sample centered at 200.5 cm uses material from 189 to 212 cm, and so is plotted with a broad symbol that spans this range.

To calculate pH from our $\delta^{11}B$ data, we use the fractionation factor (α_B) of 27.2‰ [*Klochko et al*., 2006] and $\delta^{11}B_{sw}$ of 39.61‰ [*Foster et al*., 2010], and assume temperature, salinity, and pressure at our core site of 0 °C, 35, and 3600 dbar, respectively (which gives pK_B of 8.71) [*Dickson*, 1990; *Rae et al*., 2011]. Note that likely changes to these parameters over the deglaciation at our site have little influence on the $\delta^{11}B$ to pH conversion ($<$0.025 pH units), so our record is driven, primarily, by changes in DIC and alkalinity (see Supplementary Information). Core disturbance prevented us from making core-top $\delta^{11}B$ measurements, so we assume that the *C. wuellerstorfi* at this site accurately record bottom water $\delta^{11}B$ of $B(OH)_4^-$ (and thus pH) within analytical uncertainty of ~0.3‰ (equivalent to ~0.03 pH units), as shown in other regions [*Rae et al*., 2011].

3.4. Earth System Modeling

3.4.1. Model Description

We ran a set of sensitivity tests with the GENIE Earth system model [*Cao et al*., 2009] to examine the effect of changes in North Pacific circulation on pH and radiocarbon at our site, and atmospheric CO_2, $\delta^{13}C$, and $\Delta^{14}C$. GENIE consists of a three-dimensional non-eddy-resolving frictional geostrophic ocean circulation model, two-dimensional sea ice, and energy moisture balance atmospheric models, and incorporates representations of the marine geochemical cycling of carbon and other biologically mediated tracers [*Ridgwell et al*., 2007]. We use a 36×36 equal-area horizontal resolution and 16 vertical levels, with the same physics and ocean carbon cycle configuration as described and evaluated in *Cao et al*. [2009], except with the addition of an additional iron limitation control on marine productivity [*Annan and Hargreaves*, 2010]. Although GENIE is a low ocean resolution model of intermediate complexity, it is able to successfully capture many of the large-scale features of biogeochemical cycling in the modern ocean, including simulating inventories of anthropogenic CO_2 and CFCs consistent with observations [*Cao et al*., 2009]. Crucially for this study, GENIE simulates present-day pH and $\Delta^{14}C$ distributions in the North Pacific that are in close agreement with observations. Our experiments run under pre-industrial boundary conditions start from the end of a 20,000 year equilibrium spin-up carried out with a prescribed atmospheric pCO_2 value of 278 ppm, $\delta^{13}C$ of -6.50‰, and $\Delta^{14}C$ of 0‰.

3.4.2. Experimental Design

We ran a series of salinity-addition ("anti-hosing") experiments for the surface North Pacific to explore the geochemical consequences of deep water formation. These experiments are conceptually similar, but in an opposite sense, to the widely used methodology of freshwater hosing in the North Atlantic to simulate reduced North Atlantic Deep Water formation [*Rahmstorf et al*., 2005; *Liu et al*., 2009]. Given the relatively low resolution and idealized convection scheme of GENIE, we do not aim to constrain the magnitude or location of salinity forcing required to cause North Pacific Deep Water (NPDW) formation (though we note that NPDW formation has been shown to increase in response to Atlantic freshwater forcing in a variety of more sophisticated models) [*Krebs and Timmermann*, 2007; *Okazaki et al*., 2010; *Hu et al*., 2012]. Rather, our experiments explore the effect of stratification breakdown on deep water ^{14}C and pH, and atmospheric CO_2, and use a wide range of forcing styles and boundary conditions to test the robustness of these results. Atmospheric ^{14}C production is diagnosed consistent with the model spin-up and held constant throughout our perturbation simulations.

3.4.3. Salinity Forcing

Although several lines of evidence suggest that freshwater input to the surface of the North Pacific was reduced during HS1 and the YD (section 3.3), there are considerable uncertainties in the spatial pattern and intensity of these changes. Therefore, rather than trying to match any particular record, we simply add salinity instantaneously to the surface of the North Pacific, and run sensitivity tests with a variety of spatial patterns and magnitudes of salinity addition. These include salinity addition at a single grid cell in the east, west or middle of the North Pacific; as a uniform addition to every North Pacific cell north of 51°N; and in a pattern constrained by precipitation minus evaporation (P-E) and/or salinity changes seen in general circulation model (GCM) experiments that mimic Heinrich events in the North Atlantic [*Okazaki et al*., 2010; *Krebs and Timmermann*, 2007; *Eisenman et al*., 2009]; these tend to focus the net rainfall or salinity anomaly in the NE Pacific. For each spatial pattern, we test magnitudes of salinity forcing equivalent to −0.1, −0.3, −0.5, and −0.7 Sv, similar to the magnitudes of freshwater forcing commonly used in North Atlantic hosing experiments [*Rahmstorf et al*., 2005].

3.4.4. Glacial Boundary Conditions

In addition to running anti-hosing experiments under modern boundary conditions, we also test the effect of glacial-like boundary conditions on our model results. To nudge the GENIE model into a more glacial climate state, we reduced the radiative forcing consistent with concentrations of the major greenhouse gases (CO_2, CH_4, and N_2O of 191 ppm, 350 ppb, and 216 ppb, respectively) [*Monnin et al*., 2001; *Loulergue et al*., 2008; *Schilt et al*., 2010]. In addition, we increased the zonally averaged planetary albedo profile in the Northern Hemisphere (this version of GENIE, in not including a land surface scheme, can only account for albedo in terms of a fixed net planetary profile plus the effect of sea ice [*Edwards and Marsh*, 2005]) and increased average ocean salinity by ~1 PSU.

Some studies have suggested that intermediate depths of the North Pacific were better ventilated during the LGM or early HS1 than at present [*Keigwin*, 1998; *Duplessy et al*., 1988; *Matsumoto et al*., 2002; *Herguera et al*., 2010; *Okazaki et al*., 2010; *Jaccard and Galbraith*, 2011], and thus we run a batch of salinity-forcing experiments using a base state with enhanced North Pacific Intermediate Water. We simulate this base state by reducing the prescribed transfer of freshwater from the Atlantic to the Pacific, which in the default model implicitly accounts for the net moisture transport between these basins [*Edwards and Marsh*, 2005; *Marsh et al*., 2004]. Reducing the freshwater transfer from 0.73 to 0.57 Sv results in a shoaling of NADW in the Atlantic Ocean (as seen in the reconstructions of *Curry and Oppo* [2005], *Sarnthein et al*. [2001], and *Lynch-Stieglitz et al*. [2007]) and an increase in intermediate water ventilation in the North Pacific.

We also run experiments under a glacial base state characterized by increased deep ocean stratification driven by saltier Antarctic-formed deep waters [*Adkins et al*., 2002; *McCave et al*., 2008; *Lund et al*., 2011a, 2011b]. To simulate this base state, we enhance "brine rejection" in the Southern Ocean, by increasing the efficiency with which sea ice formation transfers salinity to the deep ocean (similar to the approach of *Bouttes et al*. [2010]). This results in an expanded volume of saltier southern-sourced water in the Atlantic and Pacific and a shoaling of NADW in the Atlantic Ocean.

4. Results

At the end of the last glacial maximum (LGM), our benthic ^{14}C data are offset below the contemporaneous atmosphere by ~460‰ or ~3400 years (Figures 3 and 4, S5). This offset is much greater than for modern

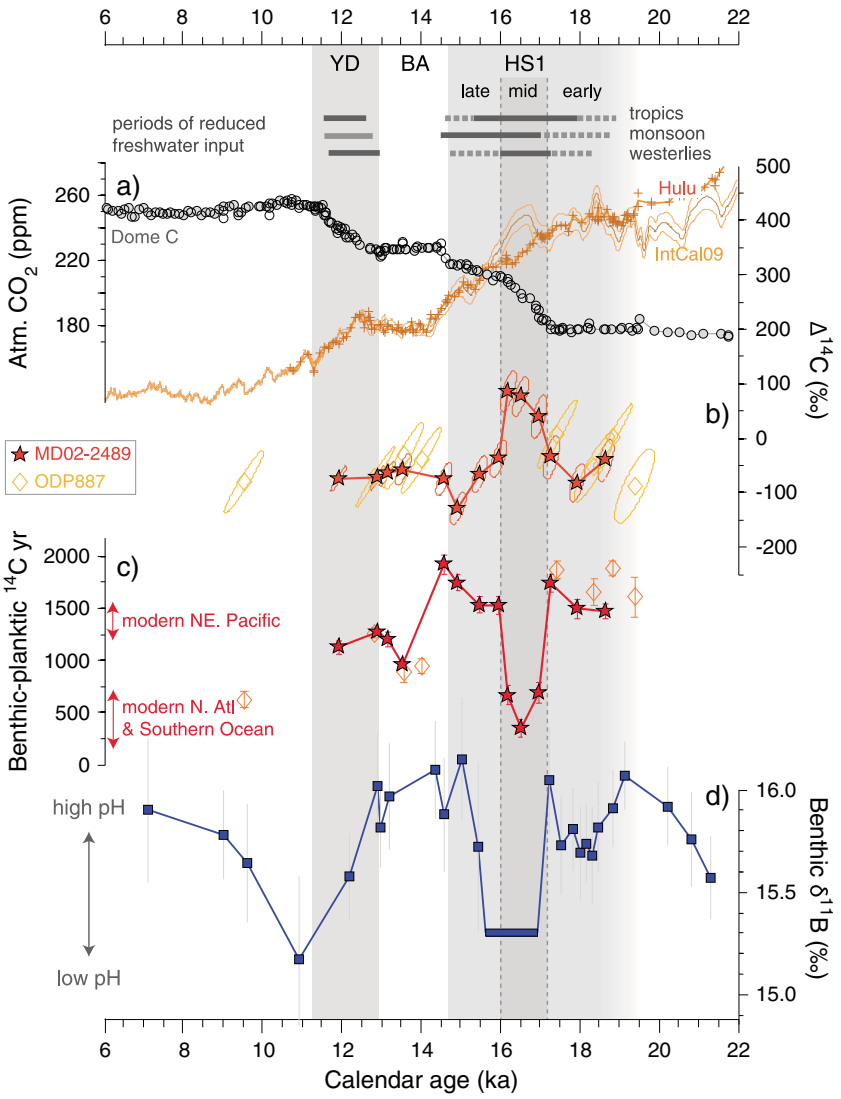

Figure 3. Deglacial radiocarbon and benthic $\delta^{11}B$ data. (a) Atmospheric CO_2 from the Dome C ice core (filled symbols from *Monnin et al.* [2001], open from *Lourantou et al.* [2010]), synchronized to the GICC05 timescale [*Lemieux-Dudon et al.*, 2010]. (b) Atmospheric $\Delta^{14}C$ from the IntCal09 compilation (yellow line) [*Reimer et al.*, 2009] and Hulu Cave H82 speleothem (orange line and crosses) [*Southon et al.*, 2012], along with benthic foraminiferal $\Delta^{14}C$ from core MD02-2489 (filled red stars and line; this study) and from adjacent core ODP 887 (open yellow diamonds) [*Galbraith et al.*, 2007] with 1 SE uncertainties. All ODP 887 ^{14}C data are plotted on the age model in Figure S4. (c) ^{14}C age difference between benthic and planktic foraminifera from core MD02-2489 (filled red stars and line; this study) and from adjacent core ODP 887 (open orange diamonds) [*Galbraith et al.*, 2007] with 1 SE error bars. (d) Boron isotope data from benthic foraminifera from core MD02-2489 with 2 SD error bars. The broad symbol in the $\delta^{11}B$ record indicates the wide temporal extent of this sample; all other samples span a similar temporal extent to the symbols. Vertical lines and bars denote divisions of deglacial climate and CO_2 change. Horizontal grey bars at the top denote periods of reduced freshwater input to the Pacific from the tropical Atlantic [*Leduc et al.*, 2007], the Westerly storm track [*Asmerom et al.*, 2010; *McGee et al.*, 2012], and the East Asian Monsoon [*Wang et al.*, 2001], based on the records in Figure 4. During mid HS1, there is a pronounced excursion in benthic $\Delta^{14}C$ and benthic-planktic ^{14}C, and a minima in $\delta^{11}B$, contemporaneous with low freshwater input and atmospheric CO_2 rise.

deep water at this site (~230‰ or ~2160 years, Figure 1c) [*Key et al.*, 2004], indicating significant isolation of DIC from the atmosphere during the LGM. Our glacial $\delta^{11}B$ data have values around 15.7‰ (Figure 3), indicating a pH of ~7.9. As water column carbonate system data (Figure 1b) [*Key et al.*, 2004] give $\delta^{11}B$ of B $(OH)_4^-$ of ~14.9‰ (Figure 1) or pH of ~7.75, our benthic $\delta^{11}B$ data suggest that the pH of the deep glacial North Pacific was ~0.15 higher than modern.

The key feature of our records occurs during the middle of Heinrich Stadial 1 (HS1) between ~17.3 and 16.0 ka. At this time, our benthic-planktic ^{14}C offsets drop from ~1750 to ~350 ^{14}C years, due to a simultaneous younging in deep waters and an increase in surface reservoir age (Figures 2–4). Our $\delta^{11}B$ record shows a negative excursion of ~0.6‰ at this time, equating to a decrease in pH of ~0.075 units, though note that $\delta^{11}B$ data resolution is low in this interval.

Following the mid-HS1 event, benthic-planktic ^{14}C offsets and $\delta^{11}B$ increase toward pre-excursion values. Then, during the Bølling-Allerød (BA 14.7–12.7 ka), benthic-planktic ^{14}C offsets decrease again, but in contrast to mid HS1, $\delta^{11}B$ data show little change. $\delta^{11}B$ displays another excursion to lower pH values during the Younger Dryas, but in contrast to HS1, ^{14}C remains relatively constant in this interval (Figure 3).

5. Discussion

5.1. Glacial and Deglacial Changes in Ventilation and Carbonate Chemistry

5.1.1. Deep Ocean Carbon Storage at the LGM

Hypotheses for lowering atmospheric CO_2 during glacial periods typically invoke increased DIC storage in the deep ocean and have often suggested the deep North Pacific as a likely store for this carbon [e.g., *Jaccard et al*., 2009]. This is supported by our benthic ^{14}C data, which have benthic-atmosphere ^{14}C ages among the oldest yet found in the deep ocean at the LGM [*Galbraith et al*., 2007; *Skinner et al*., 2010; *Sarnthein*, 2011]. These poorly ventilated deep waters would have accumulated DIC that was isolated from the atmosphere [*Sarnthein et al*., 2013], acting as an effective carbon store. The elevated pH at the LGM, implied by the comparison of our $\delta^{11}B$ data to modern water column values, suggests that any such increase in DIC storage in the deep North Pacific must have been buffered by a greater increase in alkalinity (Figure S1), consistent with regionally enhanced preservation of $CaCO_3$ [*Gebhardt et al*., 2008; *Anderson et al*., 2008]. Mechanisms that could lead to increased deep Pacific alkalinity include a carbonate compensation response to shoaling of North Atlantic deep water [*Broecker and Peng*, 1987], increased trapping of deeply remineralized $CaCO_3$ in a more stratified deep ocean [*Hain et al*., 2010], or a decrease in the rain rate ratio of $CaCO_3$ to organic carbon due to changes in productivity [*Archer and Maier-Reimer*, 1994]. As the North Pacific lies at the end of the global overturning circulation [*Talley*, 2013], the operation of any of these processes in upstream regions would be felt at our site. Note that, even though the glacial deep North Pacific had higher pH and thus likely had lower $[CO_2]$ than modern, these waters may still act as an effective carbon reservoir that contributed to low atmospheric pCO_2. The key point in this regard is that waters likely held higher DIC, rather than the particular form (CO_2, HCO_3^-, or CO_3^{2-}) in which this DIC existed.

5.1.2. Deep Water Formation During HS1

The major feature of our combined ^{14}C and $\delta^{11}B$ data set is the rapid excursion to young benthic radiocarbon ages and low pH during HS1 (Figures 2 and 3). We suggest that these excursions are best explained by a millennial-scale deep water formation event in the North Pacific. Our key evidence is the dramatic decrease in benthic-planktic ^{14}C offsets (Figures 2 and 3), which is readily explained by the onset of convective mixing between surface and deep waters. This will drive a younging in deep waters, as young surface waters are brought to depth, and an increase in surface reservoir ages, as older deep waters are mixed to the surface (Figure 1e). We note that in the modern ocean, deep to surface water offsets as small as ~350 ^{14}C years (as seen in our record) are only found near sites of deep water formation in the North Atlantic and Southern Ocean [*Key et al*., 2004].

Initiation of deep convection may also explain the low-pH excursion seen in $\delta^{11}B$ (see supporting information for further discussion of interpretation of $\delta^{11}B$ data). Although, in the modern ocean, newly ventilated deep water is typically associated with relatively high pH, this would not be expected upon initiation of deep water formation in a previously stratified basin. Figure 1 shows that our core site underlies a large body of water at intermediate depth (~200–2000 m) with extremely low pH, derived from remineralization of organic carbon, and maintained by minimal mixing with higher pH waters above and below. Initiation of deep convective mixing in the North Pacific would entrain the low pH signature of this water to the depth of our core site (Figure 1d). This process is also supported by benthic $\delta^{13}C$ data [*Gebhardt et al*., 2008] from the same core (Figure 4), which show a pronounced decrease at the start of this interval, and then climb to higher values

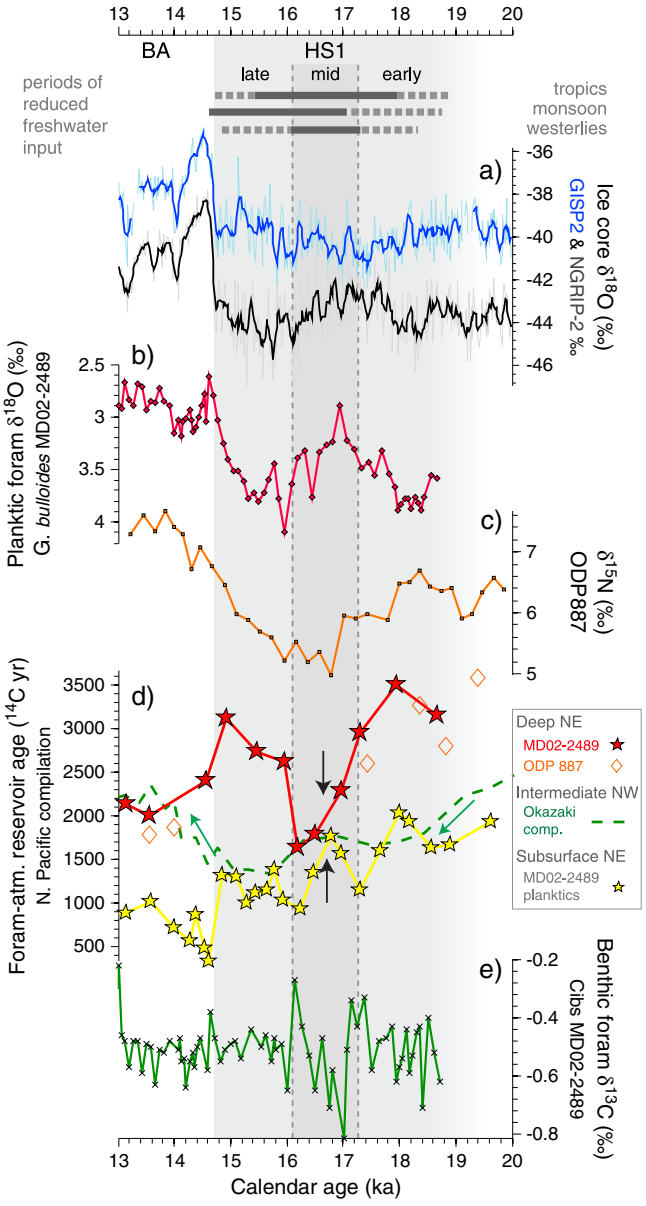

Figure 4. Supporting evidence for North Pacific deep water formation during HS1. (a) Ice core $\delta^{18}O$ from the NGRIP site in North Greenland (black) [*NGRIPmembers*, 2004] and the GISP2 site in central Greenland (blue) [*Stuiver and Grootes*, 2000]. Thin lines show 20 year resolution data, and bold lines show five-point running means. Both records are shown on the GICC05 age scale [*Rasmussen et al.*, 2008], and the NGRIP record has been offset by −2 ‰ for legibility. (b) $\delta^{18}O$ of planktic foraminifera from our core MD02-2489 [*Gebhardt et al.*, 2008]. (c) $\delta^{15}N$ data from ODP 887 [*Galbraith et al.*, 2008], shown on the age model in Figure S4. (d) Radiocarbon age difference between regional foraminiferal ^{14}C records and the contemporaneous atmosphere [*Reimer et al.*, 2009; *Southon et al.*, 2012]. Records include: benthic ^{14}C (red stars) and planktic ^{14}C (yellow stars) from MD02-2489 (this study); benthic ^{14}C from ODP 887 (open diamonds) [*Galbraith et al.*, 2007]; and benthic ^{14}C from the compilation of *Okazaki et al.* [2010] from intermediate depths of the NW Pacific. The green dashed line is a three-point running mean to the *Okazaki et al.* [2010] compilation. (e) $\delta^{13}C$ of benthic foraminifera from MD02-2489 [*Gebhardt et al.*, 2008].

during the deep water formation event. This is consistent with mixing to depth of low-$\delta^{13}C$ intermediate waters rich in remineralized carbon, which are gradually replaced by high-$\delta^{13}C$ surface waters.

Although modern waters at our site are ventilated by derivatives of Southern Ocean waters [*Reid*, 1969; *Broecker et al.*, 1998], we rule out that these data reflect circulation changes originating in the Southern Ocean: the ^{14}C excursion in the deep North Pacific precedes the major changes in Southern Ocean ^{14}C by ~1500 years, attains values ~2200 ^{14}C years younger than those at similar depths in the Southern Ocean [*Skinner et al.*, 2010], and shows a return to old ^{14}C values at 16.0 ka not observed in deep Southern Ocean ^{14}C records [*Burke and Robinson*, 2012].

The deep water formation event we infer is pronounced, but short lived. After 16 ka, we observe a return to pre-excursion benthic-planktic ^{14}C values, and an increase in $\delta^{11}B$ (Figure 3), suggesting a return to more stratified conditions. The rapid increase in benthic ^{14}C age we observe is too quick to be caused by ^{14}C radioactive decay and must result from re-penetration of old deep waters, likely from the South and East Pacific, to our core site.

Benthic-planktic ^{14}C offsets decrease again during the BA but do not reach values as low as in HS1, and $\delta^{11}B$ remains relatively high and stable (Figure 3). As this BA ^{14}C shift lags similar changes in the Southern Ocean [*Skinner et al.*, 2010; *Burke and Robinson*, 2012], and intermediate depth ^{14}C and redox records indicate stratified conditions in the upper water column [*Kennett and Ingram*, 1995; *Okazaki et al.*, 2010; *Hendy and Pedersen*, 2005] (Figure 4), we attribute this second younging to a rejuvenation in far-field ventilation rather than local vertical mixing, in agreement with previous studies [*Galbraith et al.*, 2007].

Although the YD shows a similar boron isotope excursion to that in HS1, the available benthic ^{14}C data show little

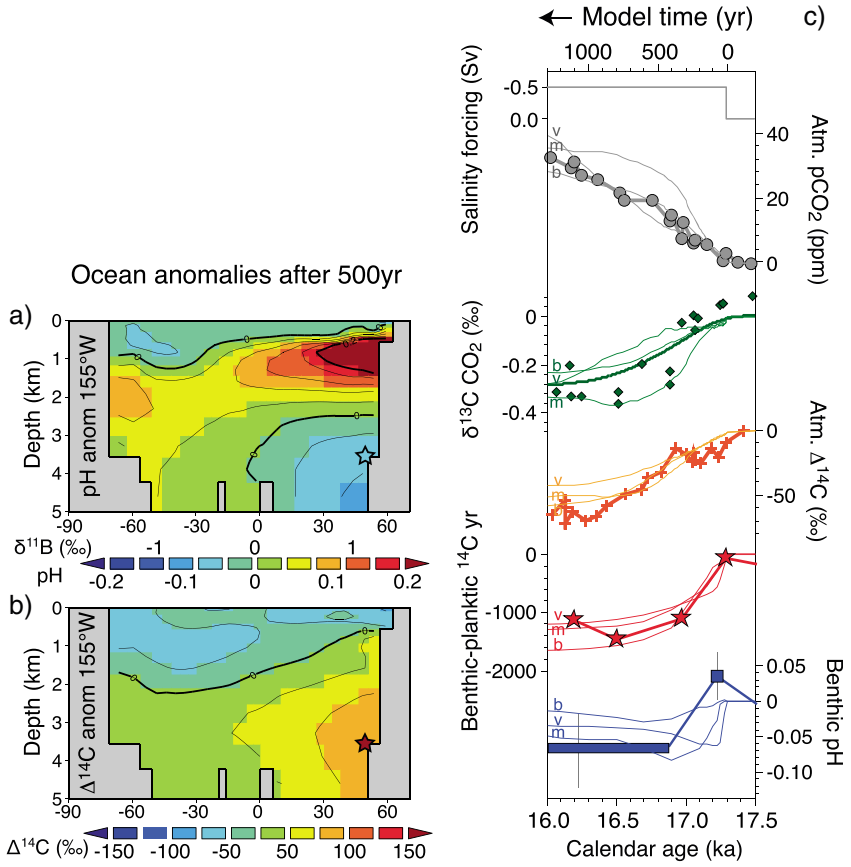

Figure 5. Summary of results from a simulation of deep convection in the North Pacific using the GENIE Earth system model. Changes seen in (a) pH and (b) $\Delta^{14}C$ after 500 years of salinity addition to the surface of the North Pacific are displayed as cross sections at the longitude of MD02-2489; the changes observed during HS1 in our $\delta^{11}B$ (pH) and $\Delta^{14}C$ data are indicated by the shading of the star. Note the decrease in pH and increase in $\Delta^{14}C$ at the depth of our core, which results from mixing with low-pH and high-$\Delta^{14}C$ waters from above. This experiment started from a modern base state and was forced by salinity addition from a point source in the middle of the North Pacific, equivalent to the removal of 0.5 Sv of freshwater ($1Sv = 10^6 m^3 s^{-1}$). (c) Time series of model results (thin lines) and data (bold lines and symbols) for atmospheric CO_2 [*Monnin et al.*, 2001; *Lourantou et al.*, 2010; *Lemieux-Dudon et al.*, 2010], atmospheric $\delta^{13}C$ [*Schmitt et al.*, 2012], atmospheric $\Delta^{14}C$ [*Southon et al.*, 2012], deep-surface ocean ^{14}C age difference, and deep ocean pH at our core site, along with the temporal evolution of the salinity forcing. Different lines refer to experiments with different model base states: m = modern (Figure 6c), v = better ventilated North Pacific intermediate water and reduced NADW formation (Figure 6f), b = saltier abyssal waters due to increased Southern Ocean brine rejection (Figure 6g). Bold line in $\delta^{13}C$ CO_2 plot is the published Monte Carlo fit to the data [*Schmitt et al.*, 2012].

change. The YD $\delta^{11}B$ excursion may thus reflect a similar mixing event to that inferred during HS1, but with a reduced deep ocean to atmosphere ^{14}C gradient (and hence less impact on deep water ^{14}C) or a spatially different pattern of mixing (see Figure). Alternatively, changes taking place in the Southern Ocean at this time may be influencing our YD $\delta^{11}B$ and ^{14}C data [*Skinner et al.*, 2010; *Burke and Robinson*, 2012]. Currently, we cannot distinguish between these scenarios, so we focus the remainder of our discussion on the better constrained HS1 event.

5.2. NPDW Formation in an Earth System Model

We test our hypothesis that the ^{14}C and $\delta^{11}B$ excursions during HS1 may be explained by deep water formation in the North Pacific using the GENIE Earth system model. Upon adding salinity to the surface of the North Pacific, we see an increase in the depth and intensity of local deep water formation, with greater magnitudes of salinity addition giving more intense and deeper convection more rapidly. North Pacific deep water formation causes a dramatic increase in $\Delta^{14}C$ in the deep NE Pacific in our model, as observed in our benthic ^{14}C data (Figures 5 and 6). This young water spreads south as a deep western boundary current, while

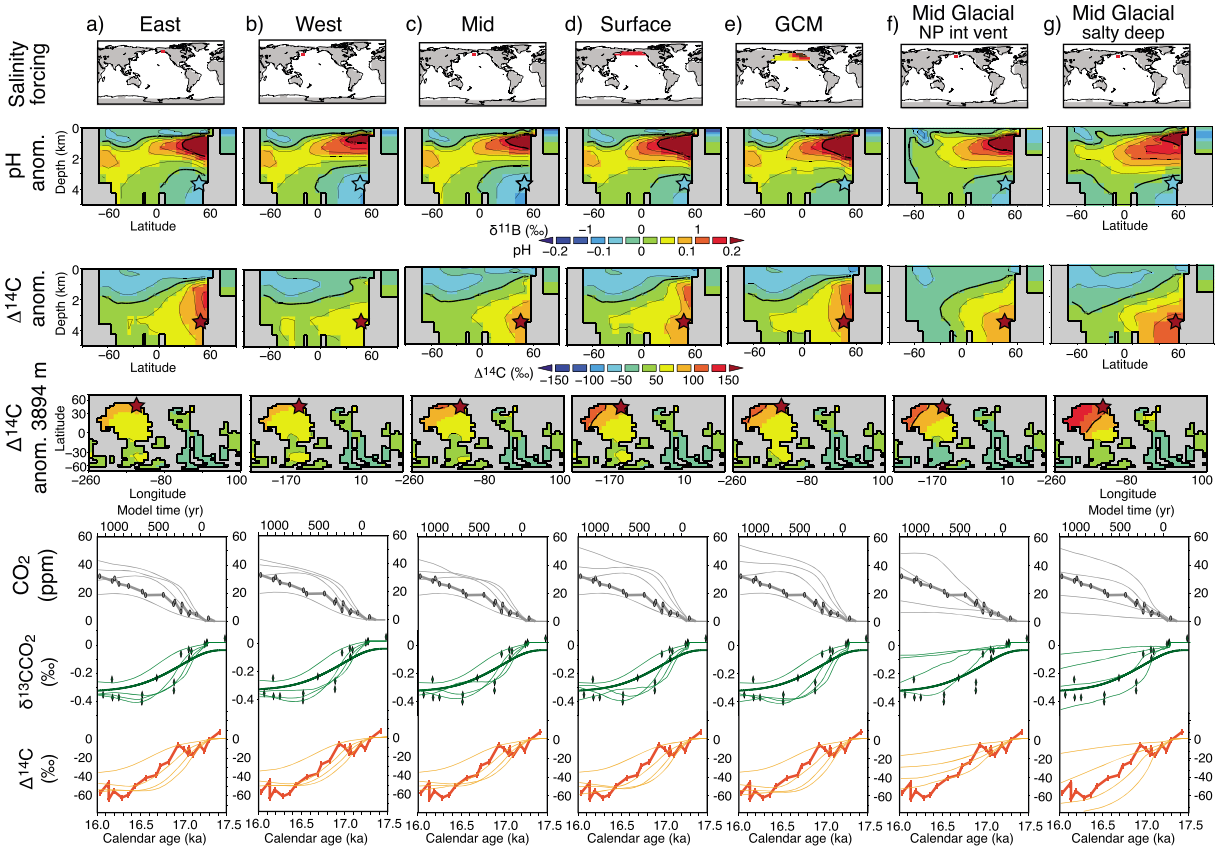

Figure 6. Earth system modeling results under (a–e) different salinity forcings and (f–g) boundary conditions. Top panel shows location of salinity addition, with shading in Figure 6e indicating varying magnitudes of salinity addition. pH and $\Delta^{14}C$ anomalies are shown after 500 years of salinity forcing equivalent to 0.5 Sv freshwater removal; the changes observed during HS1 in our $\delta^{11}B$ and $\Delta^{14}C$ data are indicated by the shading of the star. Sections and maps shown are of the closest longitude (155°W) and depth (3894 m) slices to our core. Lower panel shows time series of model results (thin lines) and early HS1 data (bold lines with symbols) for changes in atmospheric CO_2 [*Monnin et al.*, 2001; *Lourantou et al.*, 2010; *Lemieux-Dudon et al.*, 2010] and its $\delta^{13}C$ [*Schmitt et al.*, 2012] and $\Delta^{14}C$ [*Southon et al.*, 2012] composition. Time series model results are displayed for continuous salinity forcing equivalent to −0.1, −0.3, −0.5, and −0.7 Sv freshwater removal (with the largest changes corresponding to the largest forcing). Glacial boundary condition experiments include model base states with increased ventilation of North Pacific intermediate waters (f) and saltier deep waters (g), plus reduced radiative forcing, increased albedo, and increased whole ocean salinity.

waters further south and east stay relatively old (Figure 6, bottom panel). Shallower in the water column, there is a slight decrease in $\Delta^{14}C$, due to upwelling of old deep waters and a decrease in atmospheric $\Delta^{14}C$. The largest $\Delta^{14}C$ changes at our core site are seen in the experiments where deep water formation occurs nearby (e.g., Figure 6a), or in the experiments where salinity is spread over a larger area (e.g., Figure 6e), which more thoroughly mixes young waters into the deep ocean.

North Pacific deep water formation also drives a decrease in deep NE Pacific pH in our model, as seen in our $\delta^{11}B$ data (Figures 5 and 6). The pattern of pH change in the model is consistent with vertical mixing of the water column as illustrated in Figure 1d, with initially low-pH intermediate waters showing a pronounced increase in pH, and initially high-pH deep waters showing a decrease in pH. Experiments using a dye tracer confirm that the pH decrease at the depth of our core site is a result of mixing with low-pH waters from intermediate depths. However, we note that the pH decrease is transient, because continued mixing of relatively high-pH waters derived from the surface eventually overcomes the low-pH signal of intermediate waters (Figure 5c). For this reason, the most pronounced decreases in deep pH are seen when the onset of deep convection is rapid and relatively focused to a small area (Figures 6a–6c). In these experiments, the low-pH signal of intermediate waters is propagated to depth before it can be substantially diluted by mixing with high-pH surface water. Although an increase in salinity is likely to occur over a relatively large area [e.g., *Okazaki et al.*, 2010], convective mixing is, in reality, a relatively localized process [*Marshall and Schott*, 1999], so it is difficult to assess which of these forcings is most realistic.

An increase in $\Delta^{14}C$ and decrease in pH at the depth of our core are also seen in our experiments using glacial boundary conditions (Figures 5c and 6f–6g). The simulation with increased salinity in deep waters (Figure 6g) shows the largest change in $\Delta^{14}C$, as this experiment has the largest initial gradients in $\Delta^{14}C$ between the deep ocean and the atmosphere. In contrast, the decrease in pH is somewhat muted in this experiment, as the rapid penetration of newly formed deep waters to depth is inhibited by the presence of saltier bottom waters, and so more mixing between high-pH surface waters and low-pH intermediate waters occurs. In the simulation with better ventilated North Pacific intermediate waters (Figure 6f), we also see a slightly muted pH decrease, due to a reduction in the initial size and intensity of the intermediate-depth low-pH zone. However, this is in part compensated by a more rapid onset of deep water formation from this better ventilated base state.

Our modeling experiments thus confirm that local deep water formation in the North Pacific is a viable explanation for the HS1 excursions in our ^{14}C and $\delta^{11}B$ data, and show that this result is robust across a range of forcing styles and initial model base states.

5.3. Related Proxy Records from the Deglacial North Pacific

5.3.1. Ventilation Records

Although ventilation to depths >2700 m has not previously been reconstructed in the North Pacific during the deglaciation, deep water formation during HS1 is nonetheless consistent with regional proxy records (Figures 3 and 4, S5). For instance, our benthic radiocarbon data are in good agreement with those from adjacent ODP core 887 [*Galbraith et al*., 2007], but this earlier record misses the HS1 ventilation event due to lack of samples in the critical interval (orange diamonds in Figures 3 and 4, S5). At shallower depths (978–2700 m), an increase in intermediate water ventilation is seen in several radiocarbon records in the NW Pacific [*Okazaki et al*., 2010] during the whole of HS1 (~19–14.7 ka; green circles in Figures 4 and S5) and is also seen in redox records from intermediate depths of the NE Pacific [*Hendy and Pedersen*, 2005]. We note that these intermediate-depth ^{14}C records show little further younging during the 17.3–16.0 ka interval of deep water formation in mid HS1, as they are already young and well-ventilated (Figures 4 and S5). The most pronounced signal of younging on deep water formation is observed at our deep high-latitude core site, as these waters were extremely old prior to the deep water formation event, and are close to the high-latitude regions where deep water is likely to form. *Lund et al*. [2011a, 2011b] record from 2710 m on the Oregon Margin lies between these two scenarios, showing a small and gradual younging between 17.3 and 15.6 ka (purple triangles in Figure S5). This may be explained by the fact that waters at this site are quite old prior to the deep water formation event, but lie farther away from the high-latitude formation regions and the likely deep western boundary flow path of NPDW (see Figure 6 and *Okazaki et al*. [2010]).

Comparison of the high-latitude North Pacific ^{14}C records (benthic ^{14}C data from the Oregon Margin [*Lund et al*., 2011b] and the NW Pacific [*Okazaki et al*., 2010], and benthic and planktic ^{14}C data from our core), shows that regional ^{14}C gradients collapse from a spread of ~1700 ^{14}C years or 250‰ at the LGM to a range of only ~500 ^{14}C years or 60‰ during mid HS1 (Figures 4 and S5). This convergence is in contrast to a spread of ~1650 years or 150‰ in the modern North Pacific and is more typical of the modern North Atlantic [*Key et al*., 2004], providing further support for breakdown of stratification at high latitudes and local ventilation of deep waters. Furthermore, waters at ~1800 m in the South China Sea, on the likely flow path of a North Pacific western boundary current, show significant younging during HS1 (Site 17940 in *Sarnthein et al*. [2013]), and there is also some evidence for contemporaneous younging at 2800 m in the Western Equatorial Pacific [*Broecker et al*., 2008].

Recently, sediment core uranium content has been used to argue that post-glacial reventilation of the North Pacific did not occur until the BA [*Jaccard and Galbraith*, 2013]. However, authigenic uranium is not a direct proxy for ventilation and may respond to a variety of factors related to sedimentary redox conditions at various times [*Zheng et al*., 2002; *McManus et al*., 2005]. For instance, given a low redox state in deep North Pacific sediment prior to HS1, the 1200 year ventilation event we infer may cause only limited re-oxygenation of the sediment column, and any signal of this may be masked by re-precipitation of authigenic uranium following the return of poorly ventilated deep waters at ~16 ka. Furthermore, the regional pulse of organic carbon burial during the BA [*Kohfeld and Chase*, 2011] has the potential to create a sedimentary redox front [*Mangini et al*., 2001], complicating interpretation of authigenic uranium in the underlying sediments. Although we agree that re-ventilation of the North Pacific from far-field sources did occur during the BA

[*Galbraith et al*., 2007] (Figure 3), our data suggest that there was also a pulse of local deep water formation during HS1, and this is unlikely to be recorded by authigenic uranium.

5.3.2. Surface Water Signals

Additional signals of surface water stratification breakdown have been recorded in the North Pacific during HS1 but not previously linked to the process of deep water formation. $\delta^{15}N$ data from ODP 887 (Figure 4c) [*Galbraith et al*., 2008] show a broad negative excursion between ~18 and 14.7 ka, with a further decrease around 17 ka, indicating reduced nutrient utilization and reduced denitrification. Similar signals are also seen in $\delta^{15}N$ records in the NW Pacific [*Brunelle et al*., 2010] and are consistent with decreased stratification in surface waters and increased ventilation of intermediate waters. Reduced surface stratification is also reflected in planktic ^{14}C reservoir ages from our core (Figure 4d), which show an aging at ~17 ka, due to upwelling of old deep waters, and then a younging, as these old waters are replaced by younger surface waters from the south. Finally, warming is observed in a variety of surface temperature proxy records in the North Pacific [*Seki et al*., 2002; *Kiefer and Kienast*, 2005; *Gebhardt et al*., 2008; *Pak et al*., 2012; *McClymont et al*., 2012], superimposed on the general cooling of HS1 (Figure 4b—the "Atlantic-Pacific seesaw") [*Saenko et al*., 2004], as would be expected from North Pacific overturning drawing warm subtropical waters northward. Indeed, this seesaw of Atlantic and Pacific temperature changes may explain the regional differences in Greenland ice core $\delta^{18}O$ at this time (e.g., NGRIP in the north vs. GISP2 and GRIP in central Greenland; Figure 3a), given the greater proportion of North Pacific moisture at the more northerly sites [*Langen and Vinther*, 2009].

5.3.3. Productivity and Carbonate Preservation

Our $\delta^{11}B$ and ^{14}C data, and new interpretation of the deglacial ventilation of the North Pacific, offer an opportunity to re-evaluate the causes of deglacial productivity and $CaCO_3$ changes in this region. The major feature of deglacial North Pacific productivity proxy records is a pulse of export production during the BA (Figures 7d, 7e, and *Kohfeld and Chase* [2011]), at a time of relative stratification of the upper water column (Figures 4, 7a, 7b). In contrast, there is little change in productivity over the interval of inferred deep water formation in HS1 (Figures 7d, 7e and *Kohfeld and Chase* [2011]). This may be explained by the fact that productivity in the North Pacific is strongly limited by light and micronutrients [*Obata et al*., 1996; *Boyd et al*., 2007], and by consideration of likely deglacial changes in major nutrient supply.

During HS1, increased intermediate water ventilation and input of nutrient-poor subtropical waters will reduce major nutrient concentrations in the subsurface North Pacific [*Keigwin*, 1998; *Okazaki et al*., 2010]. Thus, although reduced stratification will bring more subsurface waters into the euphotic zone, these waters will have reduced nutrient contents. Furthermore, an increase in mixed layer depths will reduce the efficiency of phytoplankton productivity, due to light limitation [*Sverdrup*, 1953]. In contrast during the BA, stratification of surface waters will alleviate light limitation, while reduced intermediate water ventilation may allow subsurface nutrient concentrations to increase [*Keigwin*, 1998]. Under these conditions, wind-driven winter mixing may tap into a potent, shallow nutricline, while rapid springtime re-stratification of these warm, fresh waters [*Keigwin et al*., 1992] will promote a pronounced spring bloom, giving the pulse of export production recorded in BA sediments [*Kohfeld and Chase*, 2011]. The importance of light limitation was also recently highlighted by *Lam et al*. [2013], who demonstrated that the BA productivity spike was not associated with changes in iron input (Figure 7c). These authors also show that iron input to the North Pacific was significantly reduced following the deglaciation, which explains the fact that productivity is lower in the Holocene than the BA, despite similarly stratified conditions.

Sedimentary $CaCO_3$ content shows a minimum in the deep North Pacific during HS1 (Figures 7f, 7g) [*Gebhardt et al*., 2008; *Galbraith et al*., 2007], consistent with the decrease in deep water pH recorded by our $\delta^{11}B$ data (Figure 7h). This is followed by a spike in $CaCO_3$ content during the BA. Our $\delta^{11}B$ data indicate that deep water pH at the BA was not significantly higher than during the LGM, so this $CaCO_3$ spike cannot be primarily controlled by bottom water saturation state [c.f. *Jaccard et al*., 2005] (note that $CaCO_3$ saturation and pH are tightly coupled at any given site). Instead, the BA peak in $CaCO_3$ is likely the result of the productivity pulse at the BA, which both increases the flux of $CaCO_3$ into sediments (shown with ^{230}Th normalization by *Jaccard et al*. [2009], *Kohfeld and Chase* [2011], and *Lam et al*. [2013]) and also causes improved preservation, via rapid burial of $CaCO_3$ due to high sedimentation rates (Figure 7i). Note the lack of correspondence between $\delta^{11}B$ and carbonate preservation during the YD, which can be explained by the reduced sensitivity of sedimentary $CaCO_3$ changes to bottom water carbonate ion saturation under increased absolute $CaCO_3$ contents [*Broecker and Peng*, 1982].

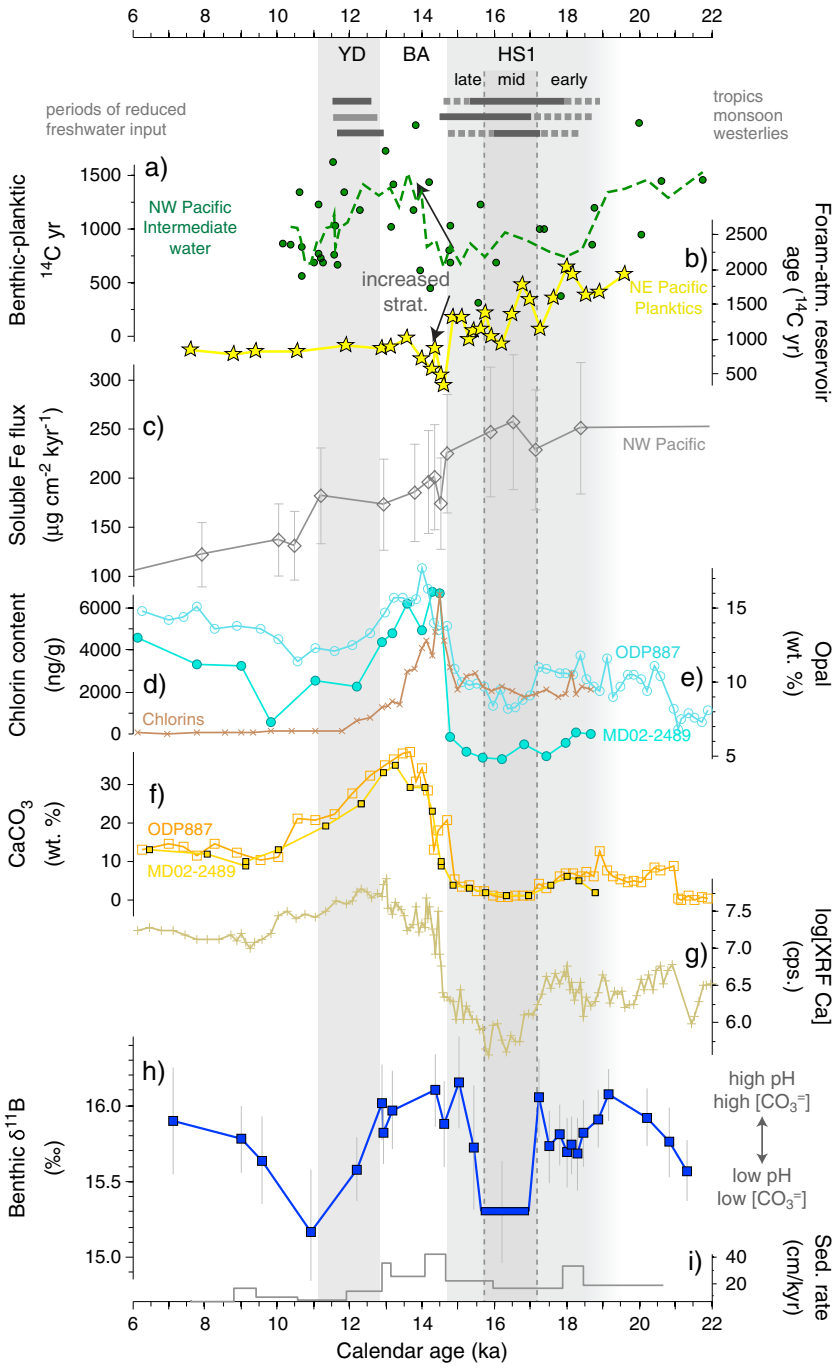

Figure 7. Deglacial productivity and carbonate preservation. (a) Benthic-planktic ^{14}C offsets from intermediate depths of the NW Pacific [*Okazaki et al.*, 2010]. Dashed line is a three-point running mean. (b) ^{14}C age difference between planktic foraminifera from MD02-2489 (this study) and the contemporaneous atmosphere. (c) Soluble iron flux to the NW Pacific, based on detrital flux measurements from *Lam et al.* [2013]. Uncertainties are 2 σ. (d) Chlorophyll pigment content from MD02-2489 (brown crosses) [*Gebhardt et al.*, 2008]. (e) Opal weight percent from MD02-2489 (filled turquoise circles) [*Gebhardt et al.*, 2008] and ODP 887 (open blue circles) [*Galbraith et al.*, 2007]. (f) $CaCO_3$ weight percent from MD02-2489 (filled yellow squares) [*Gebhardt et al.*, 2008] and ODP 887 (open orange squares) [*Galbraith et al.*, 2007]. ODP 887 records are shown on the age model in Figure S4. (g) Calcium intensity from XRF core scan of MD02-2489 [*Gebhardt et al.*, 2008], shown on a logarithmic scale. (h) δ^{11}B record from benthic foraminifera from MD02-2489 (this study). (i) Sedimentation rate from MD02-2489 (δ^{18}O-based age model in this study).

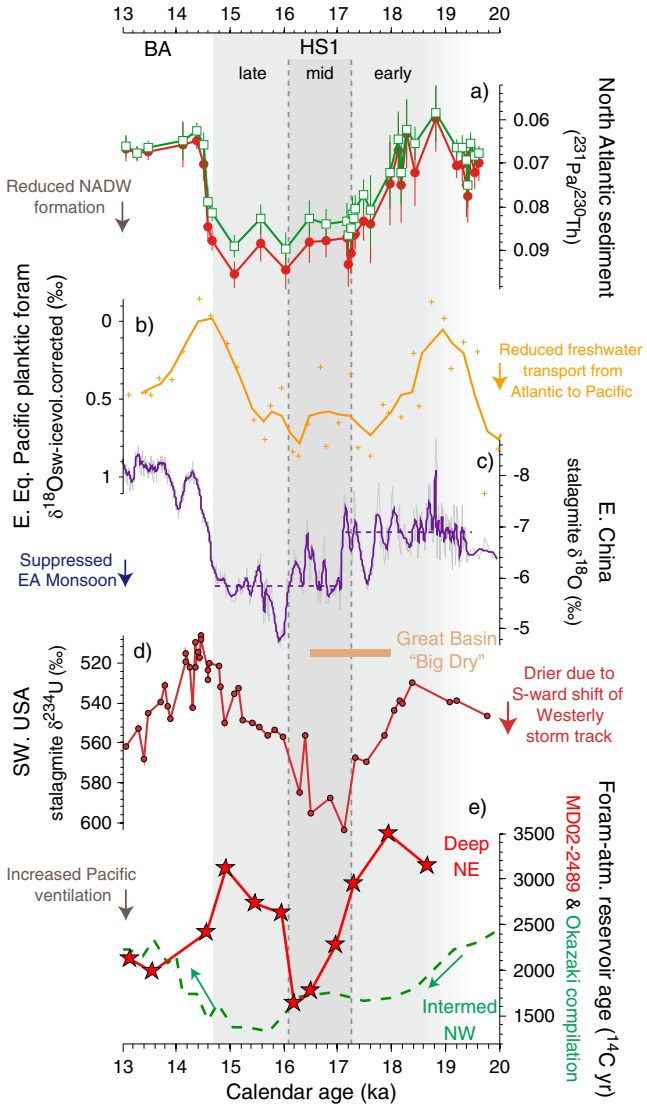

Figure 8. Causes of stratification breakdown in the North Pacific. (a) Protactinium to thorium ratios from a sediment core in the deep NW Atlantic [*McManus et al.*, 2004], which may act as a tracer for deep ocean circulation. Different lines and symbols show corrections for non-water column derived ^{230}Th and ^{231}Pa, based on ^{238}U (red circles) and ^{232}Th (green squares). (b) δ^{18}O of surface seawater in the East Equatorial Pacific, reconstructed from planktic foraminiferal δ^{18}O and $U^{k'}_{37}$ sea surface temperature and corrected for changes in global ice volume [*Leduc et al.*, 2007]. This is interpreted as a proxy for local salinity changes. Line is a three-point running mean. (c) δ^{18}O of stalagmite H82 [*Wang et al.*, 2001; *Wu et al.*, 2009; *Southon et al.*, 2012] from Hulu Cave, near Nanjing, China, a proxy for changes in the East Asian Monsoon. Bold purple line is a nine-point running mean to the data (grey line). (d) δ^{234}U of stalagmite FS2 [*Polyak et al.*, 2012], from Fort Stanton Cave, New Mexico, a proxy for local precipitation. Also shown is the time period covering the "Big Dry" interval in the Great Basin of the Western USA [*Allen and Anderson*, 1993; *McGee et al.*, 2012; *Broecker and Putnam*, 2012]. (e) Difference in ^{14}C age between benthic foraminifera and the contemporaneous atmosphere, with records from the deep NE Pacific (red stars, this study) and intermediate depths of the NW Pacific (green dashed line is a three-point running mean of the compilation of *Okazaki et al.* [2010]).

5.4. Driving Mechanisms

The onset of deep convection in the North Pacific, as hypothesized from our records, requires an increase in sea surface salinity [*Warren*, 1983; *Boyle and Keigwin*, 1987; *Talley*, 1991; *Emile-Geay et al.*, 2003; *Gebhardt et al.*, 2008]. Possible drivers include: (1) a decrease in the intensity of the East Asian monsoon [*Wang et al.*, 1999; *Wang et al.*, 2001]; (2) a southward shift of the Westerly storm track [*Allen and Anderson*, 1993; *McGee et al.*, 2012; *Polyak et al.*, 2012]; (3) a southward shift in the trade winds and Intertropical Convergence Zone (ITCZ) [*Leduc et al.*, 2007; *Pahnke et al.*, 2007]; and (4) oceanic salinity feedbacks, in response to reduced North Atlantic Deep Water formation [*Saenko et al.*, 2004]. The occurrence of such conditions during HS1 is supported by a variety of data sets (Figures 4 and 8 and *Broecker and Putnam* [2012]), as well as coupled climate model results, which commonly exhibit reduced precipitation relative to evaporation, and increased North Pacific ventilation, in response to cold HS1 conditions and reduced NADW formation in the North Atlantic [*Stocker et al.*, 1992; *Saenko et al.*, 2004; *Timmermann et al.*, 2005; *Krebs and Timmermann*, 2007; *Eisenman et al.*, 2009; *Okazaki et al.*, 2010; *Chikamoto et al.*, 2012]. North Pacific deep water formation is also aided by a closed Bering Strait during HS1 [*Hu et al.*, 2012] and may be further preconditioned by the presence of warm salty waters at depth, overlain by cold fresh waters; the mixing of these waters allows release of potential energy via thermobaricity [*Adkins et al.*, 2005]. We suggest that, in response to reduced freshwater flux at the start of the stadial (~19 ka), increased ventilation begins at intermediate depths in the NW Pacific [*Okazaki et al.*, 2010] (Figure 4e). This may prime the region for the pulse of deep water formation we observe at 17.3–16.0 ka, by drawing in high salinity waters from lower latitudes [*Stommel*, 1961]. Deep water formation may then occur as a threshold response to continued salinity forcing, or may be triggered by a further

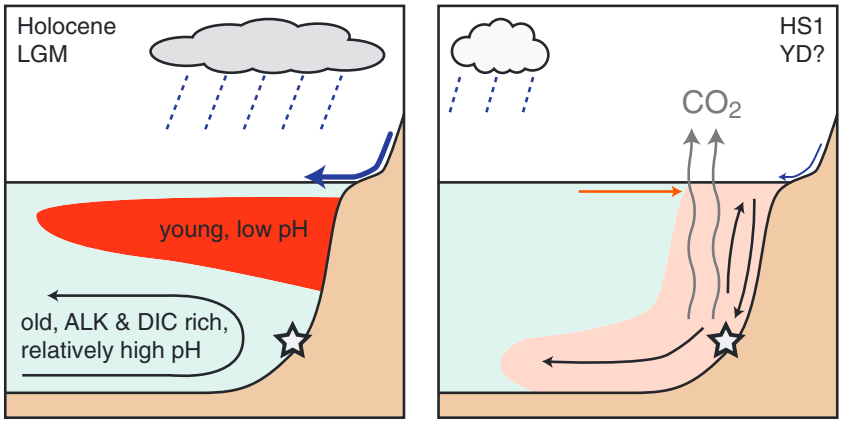

Figure 9. Cartoon of CO_2 storage and release in the North Pacific. During periods of stratification, a large volume of low pH water accumulates at intermediate depths, and old waters rich in alkalinity and DIC, and with relatively high pH, accumulate in the deep ocean. With reduced atmospheric freshwater flux, stratification breaks down and deep convective mixing occurs. This mixing causes a decrease in benthic-planktic ^{14}C offsets and a decrease in pH at our core site, and release of CO_2 from the deep ocean to the atmosphere.

decrease in East Asian Monsoon intensity [*Wang et al.*, 2001] and a southward shift in the Westerlies [*Allen and Anderson*, 1993; *McGee et al.*, 2012; *Polyak et al.*, 2012], as observed during this interval (Figures 4c and 4d).

5.5. Deglacial CO_2 Rise

The inferred North Pacific deep water formation event at 17.3–16.0 ka occurs at the same time as the first major rise in atmospheric CO_2 during the deglaciation (Figure 3) [*Monnin et al.*, 2001; *Lourantou et al.*, 2010; *Lemieux-Dudon et al.*, 2010]. Our modeling experiments show an atmospheric CO_2 rise of ~30 ppm associated with stratification breakdown in the North Pacific, very similar to the magnitude of the CO_2 rise recorded in ice core records at this time (Figures 5 and 6). This results from the exposure of carbon-rich deep waters to the surface in a region of low biological pump efficiency, leaking CO_2 from the deep ocean to the atmosphere (Figure 9). Associated with the rise of CO_2 in the model is a decline in the $\delta^{13}C$ of atmospheric CO_2 of ~0.35‰, and a drop in atmospheric $\Delta^{14}C$ of ~50‰, which are also in line with available data [*Schmitt et al.*, 2012; *Reimer et al.*, 2009; *Southon et al.*, 2012] (Figures 5 and 6).

Significant CO_2 rise, $\delta^{13}C$ fall, and $\Delta^{14}C$ fall are seen in response to North Pacific deep water formation across the range of forcing styles and boundary conditions we examine (Figure 6). The largest changes are seen in the experiments with the largest magnitudes of salinity forcing, as this causes deeper and more vigorous deep water formation, more effectively releasing CO_2 from the deep ocean to the atmosphere. In our experiments using glacial boundary conditions, changes in CO_2, $\delta^{13}C$, and $\Delta^{14}C$ are muted when relatively small salinity forcings are applied. This is because better ventilated intermediate waters (Figure 6f) mean that less DIC is initially stored at mid depths of the North Pacific, while denser deep waters (Figure 6g) inhibit the exposure of DIC stored in the abyssal North Pacific. When local mixing does penetrate the abyssal waters (under increased salinity forcing), the changes in atmospheric CO_2, $\delta^{13}C$, and $\Delta^{14}C$ in these glacial-type experiments (Figures 6f–6g) are similar to those under modern boundary conditions (Figure 6c).

Our experiments show a significant drop in atmospheric $\Delta^{14}C$ during this first period of the "mystery interval" [*Broecker and Barker*, 2007]. This is most pronounced in the simulations with salty bottom waters, as these have the largest initial gradient between old deep waters and the atmosphere. However, our results also illustrate that a significant drop in atmospheric $\Delta^{14}C$ is possible without the presence of an extremely old (>5000 ^{14}C yr) deep ocean carbon reservoir [*Broecker et al.*, 2008], as previously suggested by *Burke and Robinson* [2012].

Deep water formation in the North Pacific may thus account for a significant rise in CO_2 during early deglaciation. Although the exact timing and magnitude of this CO_2 rise will depend on other regions and processes, the previously stratified nature of the North Pacific, with old, DIC-rich waters at depth, makes it a sensitive region

from which to drive some portion of atmospheric CO_2, $\delta^{13}C$, and $\Delta^{14}C$ change. However, despite the North Pacific's likely contribution to the initial deglacial CO_2 rise, other mechanisms must also operate to cause continued CO_2 increase, and to maintain CO_2 differences between glacials and long-lived interglacials such as the Holocene. Upon restratification to a state similar to the modern (by removal of the salinity forcing in our modeling experiments), the atmospheric CO_2 anomaly decreases as DIC re-accumulates in the deep Pacific, reaching pre-excursion values within a few thousand years. Although some portion of this CO_2 drawdown may be countered by carbonate compensation [*Broecker and Peng*, 1987], it is likely that other mechanisms, such as changes in iron fertilization [*Martínez-Garcia et al*., 2009] and destratification in the Southern Ocean [*Toggweiler et al*., 2006; *Anderson et al*., 2009; *Burke and Robinson*, 2012], must also operate to offset this CO_2 fall and to achieve the full observed deglacial CO_2 rise. Rather than maintaining a steady-state difference in CO_2 between glacial and interglacial periods, we suggest that stratification breakdown in the North Pacific may act as a release mechanism for some portion of the carbon stored in the deep ocean during glacial periods.

6. Conclusions

Our deglacial radiocarbon and boron isotope records provide the first evidence of local deep water formation to 3600 m in the North Pacific. This process is reflected in a dramatic younging in benthic-planktic ^{14}C offsets, which reach ~350 years, and a decrease in $\delta^{11}B$, as low-pH waters from intermediate depths are mixed into the deep ocean. Although deep water formation to this depth has not previously been reconstructed in the North Pacific, it is supported by a range of regional proxy records. These include a collapse in regional ^{14}C gradients [*Galbraith et al*., 2007; *Okazaki et al*., 2010; *Lund et al*., 2011a, 2011b; *Sarnthein et al*., 2013], reduced surface water stratification in $\delta^{15}N$ data [e.g., *Brunelle et al*., 2010], and a regional warming [e.g., *Kiefer and Kienast*, 2005].

The ability of North Pacific deep water formation to explain our ^{14}C and $\delta^{11}B$ data is supported by our experiments with an Earth system model. Across a range of forcing styles and boundary conditions, breakdown of stratification causes a younging in ^{14}C and a decrease in pH at the depth of our core site. These experiments also demonstrate the transient nature of signals of deep water formation in a previously stratified basin: deep ocean pH initially decreases, due to input of low-pH waters from intermediate depths, and then increases, as these waters are replaced by higher pH waters from the surface ocean. Destratification does not give signals that are instantly analogous to modern deep water formation, and this should be considered when interpreting deglacial proxy data.

Our posited North Pacific deep water formation event occurs during Heinrich Stadial 1, at a time of reduced North Atlantic deep water formation and cold stadial conditions in the North Atlantic [*Sarnthein et al*., 2001]. This supports the concept of an Atlantic-Pacific seesaw of deep water formation and associated climate change [*Saenko et al*., 2004]. Deep water formation in the North Pacific requires an increase in sea surface salinity [*Emile-Geay et al*., 2003], which was likely driven by a reorganization of major rain belts in response to stadial conditions [*Broecker and Putnam*, 2012]. A southward shift of the Westerly storm track [*Polyak et al*., 2012], reduced Atlantic to Pacific freshwater transport in the tropics [*Leduc et al*., 2007], and a subdued East Asian Monsoon [*Wang et al*., 1999] may all have played a role, alongside oceanic salinity feedbacks [*Krebs and Timmermann*, 2007]. This highlights the importance of atmospheric freshwater flux in controlling deep water formation [*Eisenman et al*., 2009].

Deep water formation in the North Pacific causes significant atmospheric CO_2 rise, and a drop in atmospheric $\delta^{13}C$ and $\Delta^{14}C$ in our model, in line with atmospheric records over this period of the early deglaciation [*Monnin et al*., 2001; *Schmitt et al*., 2012; *Southon et al*., 2012]. However, upon restratification, CO_2 values return toward pre-excursion values in a few thousand years. Therefore, although North Pacific deep water formation may act as a release mechanism for some portion of a deep ocean CO_2 store, other mechanisms—likely involving the Southern Ocean—must also operate to cause continued atmospheric CO_2 rise.

Despite the ability of North Pacific deep water formation to explain our ^{14}C and $\delta^{11}B$ data, our hypothesis requires further testing. In particular, our key data are obtained from a single core, and the boron isotope data are sparse during the key interval. Although there is regional support for breakdown of stratification in shallower waters at this time [*Okazaki et al*., 2010; *Brunelle et al*., 2010], this does not provide direct evidence for deep water formation. To further test our hypothesis, more data from deep ocean cores, with high-

enough resolution to capture a ~1200 year-long event, are required. We also encourage further modeling efforts, with higher spatial resolution and different parameterizations of deep water formation, to investigate the impact of NPDW formation on paleoceanographic tracers and atmospheric CO_2.

Finally, we note that CO_2 rise during each of the last four deglaciations is associated with a Heinrich Stadial and a pronounced weak monsoon event similar to those seen during HS1 [*Cheng et al*., 2009], and we speculate that part of each of these deglacial CO_2 rises may be driven by the mechanism described here [*Gebhardt et al*., 2008]. North Pacific ventilation may thus provide an important feedback on the orbital and millennial-scale triggers of glacial terminations, with the associated CO_2 release helping to warm the planet and contribute to a full deglaciation. Overall, our work demonstrates a previously unidentified but important role for deep water formation in the North Pacific in deglacial CO_2 rise and climate variability, and highlights the fundamental influence of polar ocean stratification versus deep mixing on glacial-interglacial climate change.

Acknowledgments

The data presented in this paper are available online in supplementary data tables associated with this article, and at Pangaea and the NCDC. We thank Jess Adkins, Andrea Burke, Ian Eisenman, Jake Gebbie, Ingrid Hendy, Phoebe Lam, Naomi Levine, Tom Marchitto, Laura Robinson, Tapio Schneider, Andrew Thompson, Derek Vance, Robb Wills, and several anonymous reviewers, for constructive conversations and comments that helped shape the ideas in this manuscript. Chris Charles provided sound editorial advice. We thank IMAGES, Yvon Balut, and the crew of Marion Dufresne for obtaining a unique large-diameter sediment core that permitted numerous multiproxy studies. This work was supported by: a NERC studentship to JR; a NERC small grant (NE/I017240/1) to AR, GF, and JR; a NOAA/UCAR Climate and Global Change Postdoctoral Fellowship Program, administered by the University Corporation for Atmospheric Research, to JR; a NERC fellowship (NE/C00876X/2) to GF; and a DFG grant (Sa207/48-1) to MS and PG.

References

Adkins, J., and E. Boyle (1997), Changing atmospheric $\Delta^{14}C$ and the record of deep water, *Paleoceanography*, *12*, 337–344, doi:10.1029/97PA00379.

Adkins, J. F., A. P. Ingersoll, and C. Pasquero (2005), Rapid climate change and conditional instability of the glacial deep ocean from the thermobaric effect and geothermal heating, *Quat. Sci. Rev.*, *24*, 581–594.

Adkins, J., K. McIntyre, and D. Schrag (2002), The Salinity, Temperature, and $\delta^{18}O$ of the Glacial Deep Ocean, *Science*, *298*, 1769–1773.

Allen, B. D., and R. Y. Anderson (1993), Evidence from Western North America for Rapid Shifts in Climate During the Last Glacial Maximum, *Science*, *260*, 1920–1923.

Andersen, K. K., A. Svensson, S. J. Johnsen, S. O. Rasmussen, M. Bigler, R. Röthlisberger, U. Ruth, M. L. Siggaard-Andersen, J. Peder Steffensen, and D. Dahl-Jensen (2006), The Greenland ice core chronology 2005, 15–42 ka. Part 1: constructing the time scale, *Quat. Sci. Rev.*, *25*, 3246–3257.

Anderson, R. F., S. Ali, L. I. Bradtmiller, S. H. H. Nielsen, M. Q. Fleisher, B. E. Anderson, and L. H. Burckle (2009), Wind-Driven Upwelling in the Southern Ocean and the Deglacial Rise in Atmospheric CO_2, *Science*, *323*, 1443–1448.

Anderson, R., M. Fleisher, Y. Lao, and G. Winckler (2008), Modern $CaCO_3$ preservation in equatorial Pacific sediments in the context of late-Pleistocene glacial cycles, *Mar. Chem.*, *111*, 30–46.

Annan, J. D., and J. C. Hargreaves (2010), Efficient identification of ocean thermodynamics in a physical/biogeochemical ocean model with an iterative Importance Sampling method, *Ocean Modell.*, *32*, 205–215.

Antonov, J. I., D. Seidov, T. P. Boyer, R. A. Locarnini, A. V. Mishonov, H. E. Garcia, O. K. Baranova, M. M. Zweng, and D. R. Johnson (2010), *World Ocean Atlas 2009*, NOAA Atlas NESDIS 69, vol. 2, edited by S. Levitus, 184 pp., US Government Printing Office, Washington, D. C.

Archer, D., and E. Maier-Reimer (1994), Effect of deep-sea sedimentary calcite preservation on atmospheric CO_2 concentration, *Nature*, *367*, 260–263.

Asmerom, Y., V. J. Polyak, and S. J. Burns (2010), Variable winter moisture in the southwestern United States linked to rapid glacial climate shifts, *Nat. Geosci.*, *3*, 114–117.

Barker, S., P. Diz, M. J. Vautravers, J. Pike, G. Knorr, I. R. Hall, and W. S. Broecker (2009), Interhemispheric Atlantic seesaw response during the last deglaciation, *Nature*, *457*, 1097–1102.

Bouttes, N., D. Paillard, and D. M. Roche (2010), Impact of brine-induced stratification on the glacial carbon cycle, *Clim. Past Discuss.*, *6*, 681–710.

Boyd, P. W., et al. (2007), Mesoscale Iron Enrichment Experiments 1993–2005: Synthesis and Future Directions, *Science*, *315*, 612–617.

Boyle, E. A., and L. Keigwin (1987), North Atlantic thermohaline circulation during the past 20,000 years linked to high-latitude surface temperature, *Nature*, *330*, 35–40.

Broecker, W., and A. E. Putnam (2012), How did the hydrologic cycle respond to the two-phase mystery interval?, *Quat. Sci. Rev.*, *57*, 17–25.

Broecker, W. S. (1982), Glacial to interglacial changes in ocean chemistry, *Prog. Oceanogr.*, *11*, 151–197.

Broecker, W., and S. Barker (2007), A 190 permil drop in atmosphere's $\Delta^{14}C$ during the "Mystery Interval" (17.5 to 14.5 kyr), *Earth Planet. Sci. Lett.*, *256*, 90–99.

Broecker, W. S., and T. H. Peng (1987), The role of $CaCO_3$ compensation in the glacial to interglacial atmospheric CO_2 change, *Global Biogeochem. Cycles*, *1*, 15–29, doi:10.1029/GB001i001p00015.

Broecker, W. S., and T.-H. Peng (1982), *Tracers in the Sea*, pp. 169, Lamont-Doherty Geological Observatory of Columbia University, Palisades, New York.

Broecker, W. S., D. M. Peteet, and D. Rind (1985), Does the ocean–atmosphere system have more than one stable mode of operation?, *Nature*, *315*, 21–26.

Broecker, W., S. Peacock, S. Rubin, S. Walker, R. Weiss, E. Fahrbach, M. Schroeder, U. Mikolajewicz, C. Heinze, and R. Key (1998), How much deep water is formed in the Southern Ocean?, *J. Geophys. Res.*, *103*, 833–15.

Broecker, W., E. Clark, and S. Barker (2008), Near constancy of the Pacific Ocean surface to mid-depth radiocarbon-age difference over the last 20 kyr, *Earth Planet. Sci. Lett.*, *274*, 322–326.

Brunelle, B. G., D. M. Sigman, S. L. Jaccard, L. D. Keigwin, B. Plessen, G. Schettler, M. S. Cook, and G. H. Haug (2010), Glacial/interglacial changes in nutrient supply and stratification in the western subarctic North Pacific since the penultimate glacial maximum, *Quat. Sci. Rev.*, *29*, 2579–2590.

Burke, A., and L. F. Robinson (2012), The Southern Ocean's Role in Carbon Exchange During the Last Deglaciation, *Science*, *335*, 557–561.

Cao, L., M. Eby, A. Ridgwell, K. Caldeira, D. Archer, A. Ishida, F. Joos, K. Matsumoto, U. Mikolajewicz, and A. Mouchet (2009), The role of ocean transport in the uptake of anthropogenic CO2, *Biogeosciences*, *6*, 375–390.

Catanzaro, E., C. Champion, E. Garner, G. Marinenko, K. Sappenfield, and W. Shields (1970), *Boric Acid: Isotopic and Assay Standard Reference Materials,*, NBS (US) Spec. Publ., vol. 260, pp. 1–70.

Cheng, H., R. L. Edwards, W. S. Broecker, G. H. Denton, X. Kong, Y. Wang, R. Zhang, and X. Wang (2009), Ice Age Terminations, *Science*, *326*, 248–252.

Chikamoto, M. O., L. Menviel, A. Abe-Ouchi, R. Ohgaito, A. Timmermann, Y. Okazaki, N. Harada, A. Oka, and A. Mouchet (2012), Variability in North Pacific intermediate and deep water ventilation during Heinrich events in two coupled climate models, *Deep Sea Res. Part II*, *61*, 114–126.

Curry, W., and D. Oppo (2005), Glacial water mass geometry and the distribution of $\delta^{13}C$ of DIC in the western Atlantic Ocean, *Paleoceanography*, *20*, PA1017, doi:10.1029/2010PA002085.

Denton, G., R. Anderson, J. Toggweiler, R. Edwards, J. Schaefer, and A. Putnam (2010), The last glacial termination, *Science*, *328*, 1652–1656.

Dickson, A. G. (1990), Thermodynamics of the dissociation of boric acid in synthetic seawater from 273.15 to 318.15 K, *Deep Sea Res. Part I*, *37*, 755–766.

Dickson, A. G., C. L. Sabine, and J. R. Christian (2007), *Guide to best practices for ocean CO_2 measurements*, PICES Special Publication, vol. 3, pp. 191.

Duplessy, J., N. Shackleton, R. Fairbanks, L. Labeyrie, D. Oppo, and N. Kallel (1988), Deepwater source variations during the last climatic cycle and their impact on the global deepwater circulation, *Paleoceanography*, *3*, 343–360, doi:10.1029/PA003i003p00343.

Edwards, N. R., and R. Marsh (2005), Uncertainties due to transport-parameter sensitivity in an efficient 3-D ocean-climate model, *Clim. Dyn.*, *24*, 415–433.

Eisenman, I., C. M. Bitz, and E. Tziperman (2009), Rain driven by receding ice sheets as a cause of past climate change, *Paleoceanography*, *24*, PA4209, doi:10.1029/2009PA001778.

Emile-Geay, J., and G. Madec (2008), Geothermal heating, diapycnal mixing and the abyssal circulation, *Ocean Sci. Discuss.*, *5*, 281–325.

Emile-Geay, J., M. A. Cane, N. Naik, R. Seager, A. C. Clement, and A. van Geen (2003), Warren revisited: Atmospheric freshwater fluxes and Why is no deep water formed in the North Pacific, *J. Geophys. Res.*, *108*(C6), 3178, doi:10.1029/2001JC001058.

EPICA (2004), Eight glacial cycles from an Antarctic ice core, *Nature*, *429*, 623–628.

Ferreira, D., J. Marshall, and J.-M. Campin (2010), Localization of deep water formation: Role of atmospheric moisture transport and geometrical constraints on ocean circulation, *J. Clim.*, *23*, 1456–1476.

Fischer, H., F. Fundel, U. Ruth, B. Twarloh, A. Wegner, R. Udisti, S. Becagli, E. Castellano, A. Morganti, and M. Severi (2007), Reconstruction of millennial changes in dust emission, transport and regional sea ice coverage using the deep EPICA ice cores from the Atlantic and Indian Ocean sector of Antarctica, *Earth Planet. Sci. Lett.*, *260*, 340–354.

Fletcher, M.-S., and P. I. Moreno (2011), Zonally symmetric changes in the strength and position of the Southern Westerlies drove atmospheric CO_2 variations over the past 14 k.y, *Geology*, *39*, 419–422.

Foster, G. (2008), Seawater pH, pCO_2 and $[CO_3^{=}]$ variations in the Caribbean Sea over the last 130 kyr: A boron isotope and B/Ca study of planktic foraminifera, *Earth Planet. Sci. Lett.*, *271*, 254–266.

Foster, G. L., P. A. E. Pogge von Strandmann, and J. W. B. Rae (2010), Boron and magnesium isotopic composition of seawater, *Geochem. Geophys. Geosyst.*, *11*, Q08015, doi:10.1029/2010GC003201.

Foster, G. L., B. Hönisch, G. Paris, G. S. Dwyer, J. W. Rae, T. Elliott, J. Gaillardet, N. G. Hemming, P. Louvat, and A. Vengosh (2013), Interlaboratory comparison of boron isotope analyses of boric acid, seawater and marine $CaCO_3$ by MC-ICPMS and NTIMS, *Chem. Geol.*, *358*, 1–14.

François, R., M. A. Altabet, E. F. Yu, D. M. Sigman, M. P. Bacon, M. Frank, G. Bohrmann, G. Bareille, and L. D. Labeyrie (1997), Contribution of Southern Ocean surface-water stratification to low atmospheric CO_2 concentrations during the last glacial period, *Nature*, *389*, 929–936.

Galbraith, E. D., S. L. Jaccard, T. F. Pedersen, D. M. Sigman, G. H. Haug, M. Cook, J. R. Southon, and R. François (2007), Carbon dioxide release from the North Pacific abyss during the last deglaciation, *Nature*, *449*, 890–893.

Galbraith, E. D., M. Kienast, S. L. Jaccard, T. F. Pedersen, B. G. Brunelle, D. M. Sigman, and T. Kiefer (2008), Consistent relationship between global climate and surface nitrate utilization in the western subarctic Pacific throughout the last 500 ka, *Paleoceanography*, *23*, PA2212, doi:10.1029/2007PA001518.

Gebhardt, H., M. Sarnthein, P. M. Grootes, T. Kiefer, H. Kuehn, F. Schmieder, and U. Röhl (2008), Paleonutrient and productivity records from the subarctic North Pacific for Pleistocene glacial terminations I to V, *Paleoceanography*, *23*, PA4212, doi:10.1029/2007PA001513.

Hain, M., D. Sigman, and G. Haug (2010), Carbon dioxide effects of Antarctic stratification, North Atlantic Intermediate Water formation, and subantarctic nutrient drawdown during the last ice age: Diagnosis and synthesis in a geochemical box model, *Global Biogeochem. Cycles*, *24*, GB4023, doi:10.1029/2010GL046158.

Haug, G. H., and D. M. Sigman (2009), Palaeoceanography: Polar twins, *Nat. Geosci.*, *2*, 91–92.

Hendy, I. L., and J. P. Kennett (2000), Dansgaard-Oeschger cycles and the California Current System: Planktonic foraminiferal response to rapid climate change in Santa Barbara Basin, Ocean Drilling Program hole 893A, *Paleoceanography*, *15*, 30–42, doi:10.1029/1999PA000413.

Hendy, I., and T. Pedersen (2005), Is pore water oxygen content decoupled from productivity on the California Margin? Trace element results from Ocean Drilling Program Hole 1017E, San Lucia slope, California, *Paleoceanography*, *20*, PA4026, doi:10.1029/2004PA001123.

Herguera, J. C., T. Herbert, M. Kashgarian, and C. Charles (2010), Intermediate and deep water mass distribution in the Pacific during the Last Glacial Maximum inferred from oxygen and carbon stable isotopes, *Quat. Sci. Rev.*, *29*, 1228–1245.

Hu, A., G. A. Meehl, W. Han, A. Abe-Ouchi, C. Morrill, Y. Okazaki, and M. O. Chikamoto (2012), The Pacific-Atlantic seesaw and the Bering Strait, *Geophys. Res. Lett.*, *39*, L03702, doi:10.1029/2011GL050567.

Hutchinson, I., T. S. James, P. J. Reimer, B. D. Bornhold, and J. J. Clague (2004), Marine and limnic radiocarbon reservoir corrections for studies of late- and postglacial environments in Georgia Basin and Puget Lowland, British Columbia, Canada and Washington, USA, *Quat. Res.*, *61*, 193–203.

Jaccard, S., and E. Galbraith (2013), Direct ventilation of the North Pacific did not reach the deep ocean during the last deglaciation, *Geophys. Res. Lett.*, *40*, 1–5, doi:10.1029/2012GL054118.

Jaccard, S. L., and E. D. Galbraith (2011), Large climate-driven changes of oceanic oxygen concentrations during the last deglaciation, *Nat. Geosci.*, *5*, 151–156.

Jaccard, S. L., G. H. Haug, D. M. Sigman, T. F. Pedersen, H. R. Thierstein, and U. Rohl (2005), Glacial/Interglacial Changes in Subarctic North Pacific Stratification, *Science*, *308*, 1003–1006.

Jaccard, S., E. Galbraith, D. Sigman, G. Haug, R. François, T. Pedersen, P. Dulski, and H. Thierstein (2009), Subarctic Pacific evidence for a glacial deepening of the oceanic respired carbon pool, *Earth Planet. Sci. Lett.*, *277*, 156–165.

Johnsen, S. J., et al. (1997), The $\delta^{18}O$ record along the Greenland Ice Core Project deep ice core and the problem of possible Eemian climatic instability, *J. Geophys. Res.*, *102*, 26,397–26,410, doi:10.1029/97JC00167.

Keigwin, L. D. (1998), Glacial-age hydrography of the far northwest Pacific Ocean, *Paleoceanography*, *13*, 323–339, doi:10.1029/98PA00874.

Keigwin, L. D. (2004), Radiocarbon and stable isotope constraints on Last Glacial Maximum and Younger Dryas ventilation in the western North Atlantic, *Paleoceanography*, *19*, PA4012, doi:10.1029/2004PA001029.

Keigwin, L. D., G. A. Jones, and P. N. Froelich (1992), A 15,000 year paleoenvironmental record from Meiji Seamount, far northwestern Pacific, *Earth Planet. Sci. Lett.*, *111*, 425–440.

Kennett, J. P., and B. L. Ingram (1995), A 20,000-year record of ocean circulation and climate change from the Santa Barbara basin, *Nature*, *377*, 510–514.

Key, R. M., A. Kozyr, C. L. Sabine, K. Lee, R. Wanninkhof, J. L. Bullister, R. A. Feely, F. J. Millero, C. Mordy, and T.-H. Peng (2004), A global ocean carbon climatology: Results from Global Data Analysis Project (GLODAP), *Global Biogeochem. Cycles*, *18*, GB4031, doi:10.1029/2004GB002247.

Kiefer, T., and M. Kienast (2005), Patterns of deglacial warming in the Pacific Ocean: a review with emphasis on the time interval of Heinrich event 1, *Quat. Sci. Rev.*, *24*, 1063–1081.

Kiefer, T., M. Sarnthein, H. Erlenkeuser, P. M. Grootes, and A. P. Roberts (2001), North Pacific Response to Millennial-Scale Changes in Ocean Circulation Over the Last 60 kyr, *Paleoceanography*, *16*, 179–189, doi:10.1029/2000PA000545.

Kiefer, T., S. Lorenz, M. Schulz, G. Lohmann, M. Sarnthein, and H. Elderfield (2002), Response of precipitation over Greenland and the adjacent ocean to North Pacific warm spells during Dansgaard-Oeschger stadials, *Terra Nova*, *14*, 295–300.

Klochko, K., A. J. Kaufman, W. Yao, R. H. Byrne, and J. A. Tossell (2006), Experimental measurement of boron isotope fractionation in seawater, *Earth Planet. Sci. Lett.*, *248*, 276–285.

Knox, F., and M. B. McElroy (1984), Changes in atmospheric CO_2: Influence of the marine biota at high latitude, *J. Geophys. Res.*, *89*, 4629–4637, doi:10.1029/JD089iD03p04629.

Kohfeld, K. E., and Z. Chase (2011), Controls on deglacial changes in biogenic fluxes in the North Pacific Ocean, *Quat. Sci. Rev.*, *30*, 3350–3363.

Krebs, U., and A. Timmermann (2007), Tropical air-sea interactions accelerate the recovery of the Atlantic meridional overturning circulation after a major shutdown, *J. Clim.*, *20*, 4940–4956.

Lam, P. J., L. F. Robinson, J. Blusztajn, C. Li, M. S. Cook, J. F. McManus, and L. D. Keigwin (2013), Transient stratification as the cause of the North Pacific productivity spike during deglaciation, *Nat. Geosci.*, *6*, 622–626.

Langen, P., and B. Vinther (2009), Response in atmospheric circulation and sources of Greenland precipitation to glacial boundary conditions, *Clim. Dyn.*, *32*, 1035–1054.

Leduc, G., L. Vidal, K. Tachikawa, F. Rostek, C. Sonzogni, L. Beaufort, and E. Bard (2007), Moisture transport across Central America as a positive feedback on abrupt climatic changes, *Nature*, *445*, 908–911.

Lee, K., T.-W. Kim, R. H. Byrne, F. J. Millero, R. A. Feely, and Y.-M. Liu (2010), The universal ratio of boron to chlorinity for the North Pacific and North Atlantic oceans, *Geochim. Cosmochim. Acta*, *74*, 1801–1811.

Lemieux-Dudon, B., E. Blayo, J.-R. Petit, C. Waelbroeck, A. Svensson, C. Ritz, J.-M. Barnola, B. M. Narcisi, and F. Parrenin (2010), Consistent dating for Antarctic and Greenland ice cores, *Quat. Sci. Rev.*, *29*, 8–20.

Liu, Z., et al. (2009) Transient Simulation of Last Deglaciation with a New Mechanism for Bolling-Allerod Warming, *Science*, *325*, 310–314.

Loulergue, L., A. Schilt, R. Spahni, V. Masson-Delmotte, T. Blunier, B. Lemieux, J.-M. Barnola, D. Raynaud, T. F. Stocker, and J. Chappellaz (2008), Orbital and millennial-scale features of atmospheric CH_4 over the past 800,000 years, *Nature*, *453*, 383–386.

Lourantou, A., J. V. Lavric, P. Köhler, J.-M. Barnola, D. Paillard, E. Michel, D. Raynaud, and J. Chappellaz (2010), Constraint of the CO_2 rise by new atmospheric carbon isotopic measurements during the last deglaciation, *Global Biogeochem. Cycles*, *24*, GB2015, doi:10.1029/2009GB003545.

Lund, D., J. Adkins, and R. Ferrari (2011a), Abyssal Atlantic circulation during the Last Glacial Maximum: Constraining the ratio between transport and vertical mixing, *Paleoceanography*, *26*, PA1213, doi:10.1029/2010PA001938.

Lund, D. C., A. C. Mix, and J. Southon (2011b), Increased ventilation age of the deep northeast Pacific Ocean during the last deglaciation, *Nat. Geosci.*, *4*, 771–774.

Lynch-Stieglitz, J., et al. (2007), Atlantic Meridional Overturning Circulation During the Last Glacial Maximum, *Science*, *316*, 66–69.

Magana, A. L., J. R. Southon, J. P. Kennett, E. B. Roark, M. Sarnthein, and L. D. Stott (2010), Resolving the cause of large differences between deglacial benthic foraminifera radiocarbon measurements in Santa Barbara Basin, *Paleoceanography*, *115*, PA4102, doi:10.1029/2010PA002011.

Mangini, A., M. Jung, and S. Laukenmann (2001), What do we learn from peaks of uranium and of manganese in deep sea sediments?, *Mar. Geol.*, *177*, 63–78.

Marsh, R., A. Yool, T. M. Lenton, M. Y. Gulamali, N. R. Edwards, J. G. Shepherd, M. Krznaric, S. Newhouse, and S. J. Cox (2004), Bistability of the thermohaline circulation identified through comprehensive 2-parameter sweeps of an efficient climate model, *Clim. Dyn.*, *23*, 761–777.

Marshall, J., and F. Schott (1999), Open-ocean convection: Observations, theory, and models, *Rev. Geophys.*, *37*, 1–64, doi:10.1029/98RG02739.

Martínez-Garcia, A., A. Rosell-Melé, W. Geibert, R. Gersonde, P. Masqué, V. Gaspari, and C. Barbante (2009), Links between iron supply, marine productivity, sea surface temperature, and CO2 over the last 1.1 Ma, *Paleoceanography*, *24*, PA1207, doi:10.1029/2008PA001657.

Matsumoto, K., T. Oba, J. Lynch-Stieglitz, and H. Yamamoto (2002), Interior hydrography and circulation of the glacial Pacific Ocean, *Quat. Sci. Rev.*, *21*, 1693–1704.

McCave, I. N., L. Carter, and I. R. Hall (2008), Glacial-interglacial changes in water mass structure and flow in the SW Pacific Ocean, *Quat. Sci. Rev.*, *27*, 1886–1908.

McClymont, E. L., R. S. Ganeshram, L. E. Pichevin, H. M. Talbot, B. E. Dongen, R. C. Thunell, A. M. Haywood, J. S. Singarayer, and P. J. Valdes (2012), Sea-surface temperature records of Termination 1 in the Gulf of California: Challenges for seasonal and interannual analogues of tropical Pacific climate change, *Paleoceanography*, *27*, PA2202, doi:10.1029/2011PA002226.

McGee, D., J. Quade, R. L. Edwards, W. S. Broecker, H. Cheng, P. W. Reiners, and N. Evenson (2012), Lacustrine cave carbonates: Novel archives of paleohydrologic change in the Bonneville Basin (Utah, USA), *Earth Planet. Sci. Lett.*, *351*, 182–194.

McManus, J. F., R. François, J.-M. Gherardi, L. D. Keigwin, and S. Brown-Leger (2004), Collapse and rapid resumption of Atlantic meridional circulation linked to deglacial climate changes, *Nature*, *428*, 834–837.

McManus, J., W. M. Berelson, G. P. Klinkhammer, D. E. Hammond, and C. Holm (2005), Authigenic uranium: Relationship to oxygen penetration depth and organic carbon rain, *Geochim. Cosmochim. Acta*, *69*, 95–108.

Monnin, E., A. Indermühle, A. Dällenbach, J. Flückiger, B. Stauffer, T. F. Stocker, D. Raynaud, and J.-M. Barnola (2001), Atmospheric CO2 concentrations over the last glacial termination, *Science*, *291*, 112–114.

Nakamura, T., T. Awaji, T. Hatayama, K. Akitomo, T. Takizawa, T. Kono, Y. Kawasaki, and M. Fukasawa (2000), The Generation of Large-Amplitude Unsteady Lee Waves by Subinertial K1 Tidal Flow: A Possible Vertical Mixing Mechanism in the Kuril Straits, *J. Phys. Oceanogr.*, *30*, 1601–1621.

NGRIPmembers (2004), High-resolution record of Northern Hemisphere climate extending into the last interglacial period, *Nature*, *431*, 147–151.

Nilsson, J., P. L. Langen, D. Ferreira, and J. Marshall (2013), Ocean Basin Geometry and the Salinification of the Atlantic Ocean, *J. Clim.*, *26*, 6163–6184.

Obata, A., J. Ishizaka, and M. Endoh (1996), Global verification of critical depth theory for phytoplankton bloom with climatological in situ temperature and satellite ocean color data, *J. Geophys. Res.*, *101*(C9), 20,657–20, doi:10.1029/96JC01734.

Okazaki, Y., A. Timmermann, L. Menviel, N. Harada, A. Abe-Ouchi, M. O. Chikamoto, A. Mouchet, and H. Asahi (2010), Deepwater Formation in the North Pacific During the Last Glacial Termination, *Science*, *329*, 200–204.

Pahnke, K., J. P. Sachs, L. Keigwin, A. Timmermann, and S. P. Xie (2007), Eastern tropical Pacific hydrologic changes during the past 27,000 years from D/H ratios in alkenones, *Paleoceanography*, *22*, PA4214, doi:10.1029/2007PA001468.

Pak, D. K., D. W. Lea, and J. P. Kennett (2012), Millennial scale changes in sea surface temperature and ocean circulation in the northeast Pacific, 10–60 kyr BP, *Paleoceanography*, *27*, PA1212, doi:10.1029/2011PA002238.
Pedro, J. B., T. D. van Ommen, S. O. Rasmussen, V. I. Morgan, J. Chappellaz, A. D. Moy, V. Masson-Delmotte, and M. Delmotte (2011), The last deglaciation: timing the bipolar seesaw, *Clim. Past*, *7*, 671–683, doi:10.5194/cp-7-671-2011.
Polyak, V. J., Y. Asmerom, S. J. Burns, and M. S. Lachniet (2012), Climatic backdrop to the terminal Pleistocene extinction of North American mammals, *Geology*, *40*, 1023–1026.
Rae, J. W. B., G. L. Foster, D. N. Schmidt, and T. Elliott (2011), Boron isotopes and B/Ca in benthic foraminifera: Proxies for the deep ocean carbonate system, *Earth Planet. Sci. Lett.*, *302*, 403–413.
Rahmstorf, S., et al. (2005), Thermohaline circulation hysteresis: A model intercomparison, *Geophys. Res. Lett.*, *32*, L23605, doi:10.1029/2005GL023655.
Ramsey, C. B., R. A. Staff, C. L. Bryant, F. Brock, H. Kitagawa, J. van der Plicht, G. Schlolaut, M. H. Marshall, A. Brauer, and H. F. Lamb (2012), A complete terrestrial radiocarbon record for 11.2 to 52.8 kyr BP, *Science*, *338*, 370–374.
Rasmussen, S. O., K. K. Andersen, A. Svensson, J. P. Steffensen, B. M. Vinther, H. B. Clausen, M. Siggaard-Andersen, S. J. Johnsen, L. B. Larsen, and D. Dahl-Jensen (2006), A new Greenland ice core chronology for the last glacial termination, *J. Geophys. Res.*, *111*, D06102, doi:10.1029/2005JD006079.
Rasmussen, S. O., I. K. Seierstad, K. K. Andersen, M. Bigler, D. Dahl-Jensen, and S. J. Johnsen (2008), Synchronization of the NGRIP, GRIP, and GISP2 ice cores across MIS 2 and palaeoclimatic implications, *Quat. Sci. Rev.*, *27*, 18–28.
Reid, J. L. (1969), Preliminary results of measurements of deep currents in the Pacific Ocean, *Nature*, *221*, 848.
Reid, J. L. (1997), On the total geostrophic circulation of the Pacific Ocean: Flow patterns, tracers, and transports, *Prog. Oceanogr.*, *39*, 263–352.
Reimer, P. J., et al. (2009), IntCal09 and Marine09 radiocarbon age calibration curves, 0–50,000 years cal BP, *Radiocarbon*, *51*, 1111–1150.
Ridgwell, A., J. Hargreaves, N. Edwards, J. Annan, T. Lenton, R. Marsh, A. Yool, and A. Watson (2007), Marine geochemical data assimilation in an efficient Earth System Model of global biogeochemical cycling, *Biogeosciences*, *4*, 87–104.
Robinson, L. F., J. F. Adkins, L. D. Keigwin, J. Southon, D. P. Fernandez, S.-L. Wang, and D. S. Scheirer (2005), Radiocarbon Variability in the Western North Atlantic During the Last Deglaciation, *Science*, *310*, 1469–1473.
Saenko, O. A., A. Schmittner, and A. J. Weaver (2004), The Atlantic–Pacific Seesaw, *J. Clim.*, *17*, 2033–2038.
Sarmiento, J. and J. Toggweiler (1984), A new model for the role of the oceans in determining atmospheric pCO_2, *Nature*, *308*, 621–624.
Sarmiento, J. L., N. Gruber, M. A. Brezinski, and J. P. Dunne (2004), High-latitude controls of thermocline nutrients and low latitude biological productivity, *Nature*, *427*, 56–60.
Sarnthein, M. (2011), Northern meltwater pulses, CO_2, and changes in Atlantic convection, *Science*, *331*, 156–158.
Sarnthein, M., et al. (2001), Fundamentel modes and abrupt changes in North Atlantic circulation and climate over the last 60 ky - concepts, reconstruction and numerical modeling, in *The Northern North Atlantic: A Changing Environment*, edited by P. Schäfer et al., pp. 365–410, Springer, Berlin Heidelberg.
Sarnthein, M., P. Grootes, J. Kennett, and M. Nadeau (2007), *^{14}C Reservoir Ages Show Deglacial Changes in Ocean Currents and Carbon Cycle*. Geophys. monograph, vol. 173, 175 pp., AGU, Washingtong D. C.
Sarnthein, M., B. Schneider, and P. M. Grootes (2013), Peak glacial ^{14}C ventilation ages suggest major draw-down of carbon into the abyssal ocean, *Clim. Past*, *9*, 2595–2614.
Schilt, A., et al. (2010) Atmospheric nitrous oxide during the last 140,000 years, *Earth Planet. Sci. Lett.*, *300*, 33–43.
Schlitzer, R. (2004), *Ocean data view*, Alfred Wegener Institute for Polar and Marine Research, Bermerhaven, Germany.
Schmitt, J., et al. (2012), Carbon Isotope Constraints on the Deglacial CO_2 Rise from Ice Cores, *Science*, *336*, 711–714.
Seki, O., R. Ishiwatari, and K. Matsumoto (2002), Millennial climate oscillations in NE Pacific surface waters over the last 82 kyr: New evidence from alkenones, *Geophys. Res. Lett.*, *29*(23), 2144, doi:10.1029/2002GL015200.
Shakun, J. D., P. U. Clark, F. He, S. A. Marcott, A. C. Mix, Z. Liu, B. Otto-Bliesner, A. Schmittner, and E. Bard (2012), Global warming preceded by increasing carbon dioxide concentrations during the last deglaciation, *Nature*, *484*, 49–54.
Shcherbina, A. Y., L. D. Talley, and D. L. Rudnick (2003), Direct observations of North Pacific ventilation: Brine rejection in the Okhotsk Sea, *Science*, *302*, 1952–1955.
Shen, C.-C., A. Kano, M. Hori, K. Lin, T.-C. Chiu, and G. S. Burr (2010), East Asian monsoon evolution and reconciliation of climate records from Japan and Greenland during the last deglaciation, *Quat. Sci. Rev.*, *29*, 3327–3335.
Siegenthaler, U. and T. Wenk (1984), Rapid atmospheric CO_2 variations and ocean circulation, *Nature*, *308*, 624–626.
Sigman, D. M., M. P. Hain, and G. H. Haug (2010), The polar ocean and glacial cycles in atmospheric CO_2 concentration, *Nature*, *466*, 47–55.
Skinner, L., S. Fallon, C. Waelbroeck, E. Michel, and S. Barker (2010), Ventilation of the Deep Southern Ocean and Deglacial CO_2 Rise, *Science*, *328*, 1147–1151.
Southon, J. and D. Fedje (2003), A post-glacial record of ^{14}C reservoir ages for the British Columbia coast, *Can. J. Archaeol.*, *27*, 95–111.
Southon, J., A. L. Noronha, H. Cheng, R. L. Edwards, and Y. Wang (2012), A high-resolution record of atmospheric ^{14}C based on Hulu Cave speleothem H82, *Quat. Sci. Rev.*, *33*, 32–41.
Stocker, T. F., D. G. Wright, and W. S. Broecker (1992), The influence of high-latitude surface forcing on the global thermohaline circulation, *Paleoceanography*, *7*, 529–541, doi:10.1029/92PA01695.
Stommel, H. (1961), Thermohaline convection with two stable regimes of flow, *Tellus*, *13*, 224–230.
Stuiver, M., and P. M. Grootes (2000), GISP2 oxygen isotope ratios, *Quat. Res.*, *53*, 277–284.
Svensson, A., K. K. Andersen, M. Bigler, H. B. Clausen, D. Dahl-Jensen, S. M. Davies, S. J. Johnsen, R. Muscheler, S. O. Rasmussen, and R. Röthlisberger (2006), The Greenland ice core chronology 2005, 15–42 ka. Part 2: Comparison to other records, *Quat. Sci. Rev.*, *25*, 3258–3267.
Sverdrup, H. (1953), On conditions for the vernal blooming of phytoplankton, *J. du Conseil*, *18*, 287–295.
Talley, L. D. (1991), An Okhotsk Sea water anomaly: implications for ventilation in the North Pacific, *Deep Sea Res. Part I*, *38*, 5171–5190.
Talley, L. D. (1993), Distribution and formation of North Pacific intermediate water, *J. Phys. Oceanogr.*, *23*, 517–517.
Talley, L. D. (1997), North Pacific Intermediate Water transports in the mixed water region, *J. Phys. Oceanogr.*, *27*, 1795–1803.
Talley, L. D. (2013), Closure of the global overturning circulation through the Indian, Pacific, and Southern Oceans: Schematics and transports, *Oceanography*, *26*(1), 80–97, doi:10.5670/oceanog.2013.07.
Timmermann, A., U. Krebs, F. Justino, H. Goosse, and T. Ivanochko (2005), Mechanisms for millennial-scale global synchronization during the last glacial period, *Paleoceanography*, *20*, PA4008, doi:10.1029/2004PA001090.
Toggweiler, J. R., J. L. Russell, and S. R. Carson (2006), Midlatitude westerlies, atmospheric CO_2, and climate change during the ice ages, *Paleoceanography*, *21*, PA2005, doi:10.1029/2005PA001154.
Tomczak, M., and J. S. Godfrey (1994), *Regional Oceanography: An Introduction*, Daya Publishing House, New Delhi.
Trauth, M. H., M. Sarnthein, and M. Arnold (1997), Bioturbational mixing depth and carbon flux at the seafloor, *Paleoceanography*, *12*, 517–526, doi:10.1029/97PA00722.

Tsunogai, S. (2002), The Western North Pacific Playing a Key Role in Global Biogeochemical Fluxes, *J. Oceanogr.*, *58*, 245–257.
van Heuven, S., D. Pierrot, J. W. B. Rae, E. Lewis, and D. W. R. Wallace (2009), MATLAB Program Developed for CO_2 System Calculations. ORNL/CDIAC-105b.
Van Scoy, K. A., D. B. Olson, and R. A. Fine (1991), Ventilation of North Pacific Intermediate Waters: The Role of the Alaskan Gyre, *J. Geophys. Res.*, *96*, 16,801–16,810, doi:10.1029/91JC01783.
Wang, L., M. Sarnthein, H. Erlenkeuser, J. Grimalt, P. Grootes, S. Heilig, E. Ivanova, M. Kienast, C. Pelejero, and U. Pflaumann (1999), East Asian monsoon climate during the Late Pleistocene: High-resolution sediment records from the South China Sea, *Mar. Geol. 156*, 243–282.
Wang, P., S. Clemens, L. Beaufort, P. Braconnot, G. Ganssen, Z. Jian, P. Kershaw, and M. Sarnthein (2005), Evolution and variability of the Asian monsoon system: State of the art and outstanding issues, *Quat. Sci. Rev.*, *24*, 595–629.
Wang, Y. J., H. Cheng, R. L. Edwards, Z. S. An, J. Y. Wu, C.-C. Shen, and J. A. Dorale (2001), A High-Resolution Absolute-Dated Late Pleistocene Monsoon Record from Hulu Cave, China, *Science*, *294*, 2345–2348.
Warren, B. A. (1983), Why is no deep water formed in the North Pacific?, *J. Mar. Res.*, *41*, 327–347.
Warren, B. A., and W. B. Owens (1988), Deep currents in the central subarctic Pacific Ocean, *J. Phys. Oceanogr.*, *18*, 529–551.
Wu, J. Y., Y. J. Wang, H. Cheng, and L. Edwards (2009), An exceptionally strengthened East Asian summer monsoon event between 19.9 and 17.1 ka BP recorded in a Hulu stalagmite, *Sci. China, Ser. D Earth Sci.*, *52*, 360–368.
Yasuda, I., S. Kouketsu, K. Katsumata, M. Ohiwa, Y. Kawasaki, and A. Kusaka (2002), Influence of Okhotsk Sea Intermediate Water on the Oyashio and North Pacific Intermediate Water, *J. Geophys. Res.*, *107*(C12), 3237, doi:10.1029/2001JC001037.
Zheng, Y., R. F. Anderson, A. van Geen, and M. Q. Fleisher (2002), Remobilization of authigenic uranium in marine sediments by bioturbation, *Geochim. Cosmochim. Acta*, *66*, 1759–1772.